April 2023

Analysis and Model of Sensor-less Modified Direct Torque Control Surface Permanent Magnet Synchronous Machine for Electrical Submersible Pumping Applications

Mulu Woldeyohannes
University of South Florida

Analysis and Model of Sensor-less Modified Direct Torque Control Surface Permanent Magnet Synchronous Machine for Electrical Submersible Pumping Applications

by

Mulu Woldeyohannes

A dissertation submitted in partial fulfillment
of the requirements for the degree of
Doctor of Philosophy
Department of Electrical Engineering
College of Engineering
University of South Florida

Major Professor: Wilfrido A. Moreno, Ph.D.
Ismail Uysal, Ph.D.
Chung Seop Jeong, Ph.D.
Andres Tejada, Ph.D.
Roshani O'Bryan, Ph.D.

Date of Approval:
March 21, 2023

Keywords: Surface Permanent Motor, Field Programmable Gate Array, Hardware in the Loop

Acknowledgments

First, I thank God Almighty for His faithfulness in my life and for granting me strength and a sound mind throughout the period of the program.

Second, I would like to express my gratitude to my advisor Dr. Wilfrido Moreno, who provided constant support and guidance during every step of my doctoral studies. Without his relentless instruction, this work could not have been possible. Also, I am grateful to my defense committee members: Dr. Ismail Uysal, Dr. Chung Seop Jeong, Dr. Andres Tejada, and Dr. Roshani O'Bryan.

Further, I would like to thank my employer, Baker Hughes Inc, for financial, moral, and material support, especially for allowing me to use the company lab and resource center.

Last but not least, I dedicate this work to my lovely husband Dr. Solomon Hailu, my supportive daughters, Rhema, Yoana, Ariyam, Shiloh, my brothers and my mom.

Table of Contents

List of Tables

List of Figures

List of Notations

Symbol	Definition
dq	Rotor reference frame
αβ	Stationary reference frame
xy	Stator flux reference frame
V_a, V_b, V_c	Stator phase currents (V)
i_a, i_b, i_c	Stator phase currents (A)
V_d, V_q,	d and q axis stator voltage (V)
i_d and i_q	d and q axis stator current (A)
L_d and L_q	d and q axis inductances (H)
$V_{\alpha s}$ and $V_{\beta s}$	α and β axis stator voltage (V)
$i\alpha s$ and $i\beta s$	α and β axis stator voltage (A)
Rα and Rβ	α and β axis stator resistor (μ)
Vs	Stator current(V)
Ls	Stator inductance (H)
is	Stator current (A)
Rs	Stator resistor (μ)
T	Electromagnetic torque (Nm)
ψ	Stator flux reference (Wb)
ψm	Permanent magnet flux linkage (Wb)

P	Number of pole pairs
ω	Rotor speed
Ψα and Ψβ	α and β axis stator flux linkage (Wb)
δ	Angle between the rotor and stator flux linkage
θ	Angular position

Superscript	**Definition**
*	Reference Value
^	Estimated Value

Acronym	**Definition**
ES	Electrical Submersible Pumping
VSD	Variable Speed Drive
PM	Permanent Magnet
PMM	Permanent Magnet Motor
SPMSM	Surface Mounted Permanent Magnet Synchronous Motor
SPM	Surface Mounted Permanent
IPM	Interior Mounted
IM	Induction Motor
PMSM	Permanent Magnet Synchronous Machine
AC	Alternating Current
DC	Direct Current
EMF	Electromagnetic Force
V/Hz	Volt per Hertz
FOC	Field Oriented Control

DTC	Direct Torque Control
SVM	Space Vector Modulation
PWM	Pump Pulse Width Modulated
VVI	Variable Voltage Inverter
CVI	Constant Voltage Inverter
DOL	Direct On-line
DSP	Digital Signal Processor
FPGA	Field Programmable Gate Array
HI	Hardware in the Loop
DOE	Design of Experiments
FAT	Factory Acceptance Tests
IGBT	Insulated-Gate Bipolar Transistor
SCR	Silicon-Controlled Rectifier
THD	Total Harmonic Distortion
ITHD	Voltage Total Harmonic Distortion

Abstract

This dissertation examines a novel sensor-less Direct Torque Control (DTC) strategy for Electrical Submersible Pump (ESP) systems using Surface Mounted Permanent Magnet Synchronous Motors (SPMSM) that are used for oil and gas production. As oil and gas are the two largest fuels in use today to generate energy, the technologies to improve efficiency, increase reliability and reduce carbon footprint are essential. SPMSM is one of the main motor topologies in use to improve the reliability and efficiency of ESP systems. Due to the absence of damper winding, SPMSM cannot be started using Direct On-Line (DOL) control. Instead, Variable Speed Drives (VSD) are typically used, which require power electronics convention from the power supply. Measuring or estimating the rotor position and speed for feedback to the control system is highly important. This requires a mechanical position or speed sensor. For ESP applications where the motor is located in the well thousands of feet below the surface, the physical sensor approach presents many more concerns such as reduced reliability, susceptibility to noise, and temperature sensitivity just, to name a few. It also increases the complexity, and cost of the ESP system. To avoid the disadvantage of mechanical sensors, great efforts have been made on the development of sensor-less control schemes such as Volt per Hertz(V/Hz), Field Oriented Control (FOC), and Direct Torque Control (DTC).

DTC of a Permanent Magnet Synchronous Machine (PMSM) is known to give fast and good dynamic torque response. One major problem associated with DTC drive is that the switching frequency varies with the operating condition. In ESP applications with step-up

transformers variable frequency is a big challenge. To solve this challenge, DTC schemes based on Space Vector Modulation (SVM) with fixed switching frequency have been proposed.

The objective of this dissertation is to investigate novel control strategies for the design, modeling, analysis, and implementation of sensor-less DTC- SVM SPMSM control for ESP systems. The DTC- SVM proposed strategy is focused on the design of the optimal stator voltage vector based on the error signal between the estimated electromagnetic torque and the estimated stator flux linkage values. The controller compares the estimated electromagnetic torque and stator flux linkage with their respective reference values. The comparators are used to determine demand torque, flux magnitude, and flux vector. DTC uses no current controller or motor parameters other than the stator resistance and inductance, which yields a faster torque response and lower parameter dependence.

A mathematical model of DTC- SVM SPMSM control demonstrated quick and robust torque reaction and high-efficiency performance will be developed, analyzed, and verified using a Field Programmable Gate Array (FPGA) based Hardware in the Loop (HIL) concept. The machine model considers operating conditions below and above synchronous speed. The DTC- SVM technique uses electromagnetic torque and flux as the controlled variable, where the feedback signals are obtained through flux and torque estimators.

The simulation results of the DTC- SVM SPMSM-drive system will be presented. SPMSM control model will be connected to the ESP system with a sine-wave filter, step-up transformer, and long cables. It will then be modeled and examined under different load conditions during steady-state and transient operations. Furthermore, motor performance and characteristics will be evaluated at different loads and speed conditions. A Design of Experiments (DOE) will be

conducted to confirm the designed control approaches, the robustness and effectiveness of the method, and the performance of the drive system. Finally, a trade-off analysis for System Power Quality will be performed, and the results presented.

Chapter 1: Introduction

1.1 Background

In the 20th century, the Electrical Submersible Pump (ESP) revolutionized oil and gas production. However, with the rise of unconventional oil, an upgraded ESP design became necessary in the 21st century [1]. Improving systems run-life, reliability, and efficiency became increasingly critical in both unconventional (horizontal or deviation) and conventional (traditional or vertical) fields [2]. ESP systems are notoriously complex interconnected systems that continually change in structure due to diverse operating conditions and production behaviors. ESP systems, as shown in Fig. 1.1, typically include a multiple-stage centrifugal electric submersible pump, an electrical submersible motor, and a downhole cable ranging from 1,000 ft to 10,000 ft up to 15,000 in extreme depths, connecting to a surface Variable Speed Drive (VSD) and transformers [3]. The motors have long stacks and limited diameters, typically ranging from 5 3/8" to 9 5/8", with exceptional form factors. In recent years, Permanent Magnet Synchronous Motors (PMSM) have emerged as the motor of choice for ESP due to their small volume, high efficiency, high torque, and great power density [4], [5].

ESPs are installed inside or near the production well, which means that in offshore ultra-deep-water scenarios, maintenance is prohibitive because of the need for expensive and availability of rig platforms. Application errors, assembly errors, and manufacturing defects must be avoided to make the method feasible and to avoid premature failure. One way to improve

assembly errors and manufacturing defects is through rigorous quality control, qualification tests, and operational procedures [6].

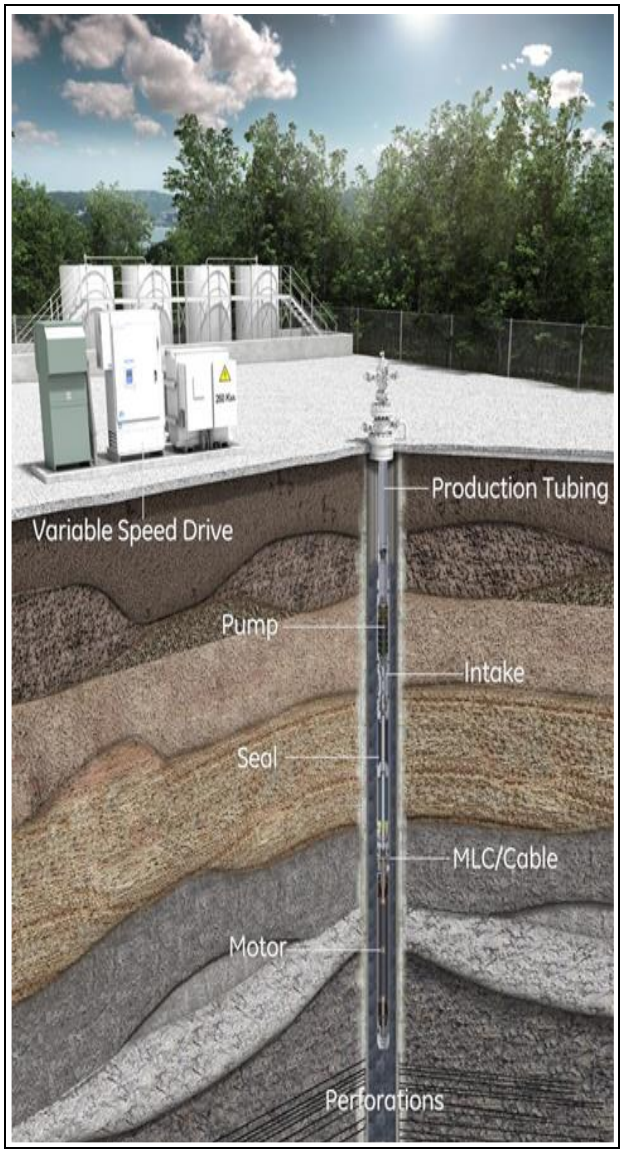

Figure 1.1 Downhole ESP Assembly

ESP manufacturers employ Factory Acceptance Tests (FATs), however, they do not fully simulate the complete ESP system behavior under real-world system operating conditions.

Additionally, some tests based on vibration analysis signals do not detect system faults when an equipment test is performed separately. For these reasons, FATs do not guarantee that an ESP system will be sufficiently robust to face the harsh environment oil field. Replacement of a failed ESP can easily run from $15,000 to $40,000 [7]. When more expensive rig costs are added, the replacement of a failed ESP becomes a significant expense. Several studies have focused on understanding the failure mechanisms to improve overall ESP system reliability [8].

According to the ESP Failure Nomenclature standard consistent with API RP 11S1 and ISO 1422 [9], most ESP failure is associated with design, manufacturing, and application. To reduce the uncertainty in prediction, run life, and reliability; system modeling, analysis, and testing play important roles.

Most modeling and analysis are available for ESP equipment such as pumps, cables, control, and motor. These may not provide a pragmatic solution to system reliability and run-life problems. A significantly large number of equipment failures are associated with system instability or miss applications [10]. In system modeling, several independent functional modules, such as inverter modules, cable modules, step-up transformer modules, pump modules, and others, play an important role in controlling PMSM [11], [12]. The combination of these simulations and analyses has allowed manufacturers and end-users to better understand the system's performance and behavior. Advanced system simulation and analysis driven by large and consistent data can improve stability, operation, and system tolerance.

1.2 Electrical Submersible Pumps (ESPs) System

Armais Arutunoff developed the first ESPs in 1916 [13]. Despite the 90 + years of worldwide application, today's typical ESP system has not changed much throughout the years.

It still uses a multistage centrifugal pump, a protector or seal section, an electric motor, a power cable, and a surface control [14]. However, the system's components' design, functionality, and material have significantly evolved, and today's systems provide highly improved capabilities compared to original ESPs [15].

Initially, all ESP operation was Direct-On-Line (DOL), i.e., a suitably rated three-phase contactor started and stopped the ESP. Because of the small rotor diameter and resulting low inertia, typical ESP starting times were less than half a second [16]. However, for high-horsepower ESPs, DOL starting produced significant inrush current and voltage sag on the power system [17]. Frequently, the power utility would impose inrush current restrictions, and solid-state soft starters, i.e., variable voltage and variable frequency, were often installed to meet those restrictions. Overzealous operators thought longer starts were better, causing the breakage of motor shafts between tandem motor sections, not at the maximum torque between the motor and the pump. Speed hunting and torsional vibrations were attributed to the negative damping characteristic of an Induction Motor (IM), where the slip is greater than the breakdown-torque slip [18]. The major problems with DOL starting were changing well productivity and operation of the pump outside its best efficiency range. With the fixed-frequency operation, the pump was incapable of compensating for this change [19].

VSD operation of ESPs was introduced in the late 1970s [20], allowing pumping at speeds that produced the well and kept the pump within its best efficiency range. Outside that range, electric costs changed little, but the reduction in the fluid produced was unacceptable. Furthermore, the VSD solved the problem of reducing inrush current during starting while still maintaining the IM in the low-slip positive-damping speed.

Three-phase, squirrel cage, alternating current IM used oil-filled since the beginning of ESP development. Being the most reliable and most efficient of conventional electric motors, they are very popular in oilfield applications. The mechanical construction of the motor has not changed since Arutunoff's time [21]. The stationary stator contains the three-phase windings connected to the electric power supply; the rotor comprises short sections keyed to the motor shaft. Improvements in the stator assembly occurred mostly in the insulation system: wire to wire, phase to phase, and phase to ground insulations. Early motors used fabrics and varnish for insulation that limited applicable motor voltages and materials and epoxy resin were used as insulators that enabled motors to have higher terminal voltages and greater powers [22]. The basic weaknesses of three-phase asynchronous induction motors are low maximum efficiency, i.e., about 85%, low power factors, high heat generation, etc. These shortcomings can be eliminated if Permanent Magnet Motors (PMMs) are used [23].

Permanent magnets are manufactured from rare-earth materials [24]. The magnets provide the necessary magnetic flux in the rotor without any outside energy requirement. The construction of the rotor and distribution of magnetic flux lines created by the permanent magnets. In comparison, to create a similar magnetic flux in an induction motor energy from the stator's magnetic field is taken to induce an electric current in the "squirrel cage" of the rotor [25]. This difference alone guarantees that PMMs are more efficient than IMs to convert electric energy to mechanical work.

1.3 Electrical and Mechanical Specification

The PMs used in PMMs are about ten times stronger than traditional ferrite magnets, so they provide an exceptionally strong magnetic flux in the motor's air gap [26]. As motor power is

proportional to the magnitude of magnetic flux, PMMs generate much greater powers than their induction-type counterparts of the same size [27]. This is seen if the power capacities of one single rotor of the two motor types are compared. The traditionally used rotor in IMs with round copper bars develops a power of five HP, improved models with shaped bars provide ten HP, whereas PM rotors reach 22 HP for the same length. This feature of PM rotors allows building shorter motors with the same power capacity; motor length and weight are reduced, as compared to IMs.

1.3.1 Operational Features

PMMs are synchronous machines so their speed does not change with the torque load. They keep their speed in the normal torque loading ranges. This behavior is shown in Table 1. 1. where the motor speed equals the synchronous speed, N_{synch} at the actual torque load. Under the same loading as an asynchronous motor.

Table 1.1 Synchronous Speed of Permanent Magnet Motor

Electrical frequency (Hz)	Motor Speed (RPM)	
	Two-Pole Motor	Four-Pole Motor
50	3,000	1,500
60	3,600	1,800
100	6,000	3,000
133	8,000	4,000
150	9,000	4,500
167	10,000	5,000

Table 1.1 (Continued)

183	11,000	5,500
200	12,000	6,000

The synchronous speed of PMMs found from Eq. (1.1) is repeated here:

$$N_{sync} = \frac{120f}{P} \quad 1.1$$

where

Nsync = synchronous speed, RPM

f = frequency, Hz

P = number of poles in the stator,

The speed of PMMs is proportional to the frequency of the electric power and inversely proportional to the number of poles in the rotor. According to their speed ranges, PMMs used in the petroleum industry can be classified into the following groups [28].

Table 1.2 Motor Operating Speed Ranges and Application

Group Speed Ranges (RPM)	**Speed Ranges (RPM)**	**Speed Ranges (RPM)**
Low Speed	100 - 1,500	PCP operations
Standard Speed	2,400 - 4,200	ESP operations
High Speed	4,200 - 6,000	ESP operations
Ultrahigh Speed	up - 12,000	Special ESP

The operation of PMMs can be described by two formulas that determine their performance. The first involves the relationship between the motor current and the torque developed and can be written as: [29]

$$T = k_1 \Phi I \quad (1.2)$$

where

T = torque developed by the motor

k_1 = conversion constant

Φ = magnetic flux developed by the PMs

I = motor current.

The other basic formula permits the calculation of the voltage (back-EMF) induced in the stator coils by the rotating PMs in the function of the rotor's angular speed; it is written as:

$$U = k_2 \Phi N \quad (1.3)$$

where

U = Induced voltage in the stator

K_2 = Conversion constant

Φ = Magnetic flux developed by the PMs

N = Motor rotational speed.

Since the magnetic flux developed by the PMs is constant, two basic conclusions can be derived from equations 1.2 and 1.3:

1. The torque developed by PMMs is directly proportional to the current taken by the motor.

2. The rotational speed of the motor changes linearly with the voltage applied to the motor.

1.3.2 High-Speed (Ultrahigh Speed) Permanent Magnet Motor

The operating speed range of Ultrahigh-speed (UHS) equipment is between 1,000 and 12,000 RPM, although their special pumps can operate at speeds up to 15,000 RPM. Because of this extremely high operating speed, the whole ESP system is significantly shorter, less than half to one-third of the length of conventional units. PMMs used in the UHS service of major manufacturers [30] have six poles and a rated speed of 10,000 RPM at a frequency of 333 Hz. Their rotors are considerably shorter than those of standard IMs and thus have a much higher power density. The heat generated by the motor's operation at such high speeds required the development of an enhanced cooling system. Cooling is provided by an active system in contrast to the passive cooling system used in IMs which consists of an oil-circulating pump and heat exchanger built into the motor base and a protector with an increased oil capacity [31].

It is also important to note that UHS ESPs have significantly better performance in low-rate and slim-hole applications. For example, the efficiency of UHS pumps producing 100 -200 BPD is greater than 50%, whereas standard-speed pumps have efficiencies typically below 40%. The higher efficiency of the UHS pumps leads to longer system run life and fewer problems associated with high pump temperatures, such as scale deposition, MLE overheating, and bearing problems [32].

1.4 Machine Technologies

1.4.1 Surface Permanent Magnet Machine (SPM)

The surface permanent magnet synchronous machine employs surface-mounted rotor magnets to achieve high torque and power densities. Such characteristics make the SPM well-suited for delivering the high starting torque required in the starter/alternator application. The SPM has difficulty achieving wide constant-power speed ranges because its back-EMF rises linearly with speed, and its phase inductances are typically too low for effective flux weakening [33]. The magnets can be placed in many ways on the rotor. The radial-field surface and interior permanent magnet are shown in Fig. 1.2 a and b respectively.

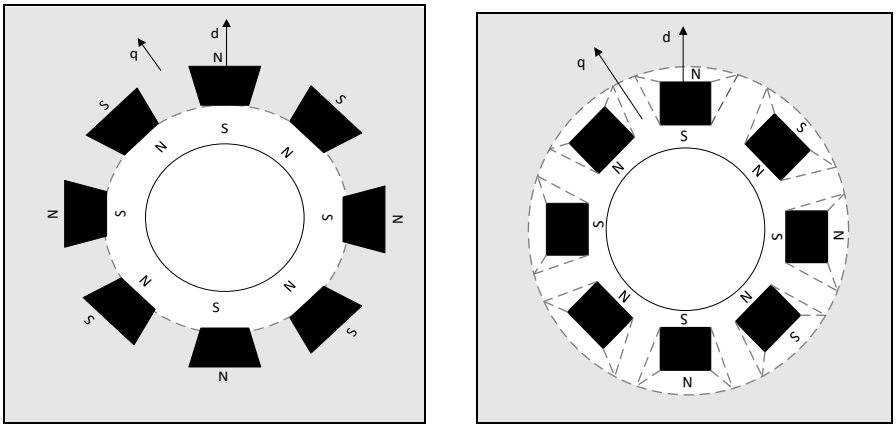

Figure 1.2 (a) Surface PM (SPM) (b) Interior PM (IPM)

1.4.2 Interior Permanent Magnet Machine (IPM)

IPM magnets are buried inside the rotor. As a result, the IPM is inherently a 'hybrid' machine with torque contributions from both the magnets and the iron saliency produced by the magnet cavities. IPM synchronous motors offer many advantages over induction motors, such as higher overall efficiency, effective use of reluctance torque, smaller losses, and compact motor size [34]. Moreover, the use of flux weakening control based on pole saliency supports a wider

range of speeds. In particular, proper balancing of the magnet strength and the rotor saliency makes it possible to achieve very wide speed ranges of constant-power operation. This is a major advantage over the SPM discussed above, further accentuated by the IPM's need for significantly less magnet material to deliver the same torque [35].

1.5 Power Converter Topology

1.5.1 Electrical System Configuration and Power Converter Topology

Direct powering of the motor from the grid or an isolated generator cannot be used to achieve adequate or proper control of the motor because it provides line voltages that are fixed in magnitude and frequency. Thus, power conversion is needed to convert fixed-line voltage signals to variable ones. This is accomplished using VSD.VSDs mainly consist of the converters, i.e., rectifier and inverter, and the dc-link components, i.e., dc inductor and dc capacitor. The rectifier converts the ac-power ac line voltages to dc power dc voltage. The most common types of rectifiers for a three-phase system are diode-rectifiers, i.e., uncontrolled rectifiers, Silicon-controlled Rectifiers (SCRs), and Insulated-gate Bipolar Transistor (IGBT) rectifiers also known as active front end. The dc-link components act like a low pass filter to smoothen out the dc power and like storage to temporarily store the dc power before it is converted back into ac power by the inverter. Depending on the modulation scheme of the inverter and the way the SCRs are being fired, the magnitude and the frequency of the drive's output voltages/currents are varied to properly control the motor.

1.5.2 Three-Phase Full Bridge Rectifiers

The most common rectifier in high-power electronic devices is the three-phase full bridge rectifier. It uses six devices, most commonly diodes or SCRs, to form the bridge. Two devices are

connected to each of the three incoming phases. One device from each phase connects to the positive DC bus, and the other to the negative bus. Each of these six devices conducts during either the positive or the negative half cycle of its respective phase. This means two pulses on each incoming phase thus in a total of six in a six-pulse converter.

The six-pulse converter has characteristics that are somewhat invariant in both control and uncontrol rectifier the distortion, depending on the manner in which it is applied. Input current distortion levels of 25% to 35% are typical. However, through misapplication or improper DC bus component sizing, the level can be much higher. Six pulse converters should not be confused with the six-step or variable voltage inverter. These are two different converters, and neither or both may be present in any given VSD.

1.5.3 Multi-Pulse Converter Rectifiers

Multi-pulse converter rectifiers are used to reduce input current harmonics in power electronic equipment. Most multi-pulse systems used today are multiple three-phase bridge rectifiers connected in parallel via phase or time-shifted power supplies. In multi-pulse systems, two pulses per phase are still achieved, thus the pulse number is always twice its input phase number.

A phase-shifted power supply is accomplished by using a phase-shifting transformer. The transformer is connected to a standard three-phase supply and through a vector combination of those three phases develops the required number of output phases. This transformer may or may not be included as a part of the VSD hardware. Care must be used to understand whether a multi-pulse VSD system requires a special or standard power supply common to a multi-pulse system is the twelve-pulse bridge, which uses six-pulse converters phase shifted by 30 degrees.

In two six pulse converters are connected to a dual wound delta/wye secondary which provides the necessary 30-degree phase shift, as shown in Fig. 1.3.

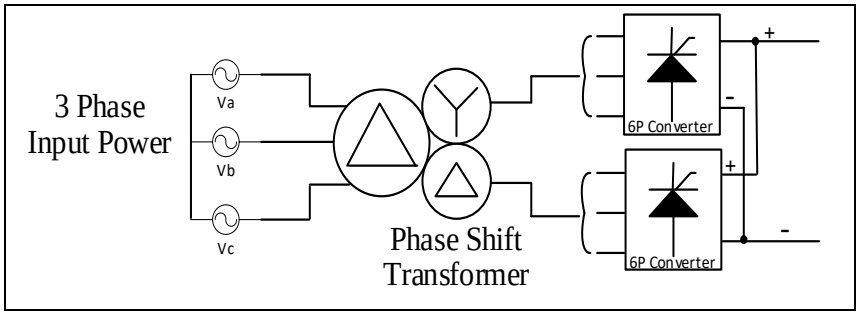

Figure 1.3 Twelve-Pulse Pulse Converter

Generally, a twelve-pulse converter can reduce input current Total Harmonic Distortion (THD) from the six-pulse average of around 30% to about 8% [36]. This is a significant reduction in THD. In cases where the short circuit system capacity is more than 20 greater than the VSD load current, the twelve-pulse converter will allow full compliance with the IEEE Std 519-1992, IEEE Recommended Practices. Requirements for Harmonic Control in Electrical Power Systems will be discussed more in standard in the applications section.

A converter with a higher pulse number will further reduce the input current distortion levels. For instance, an eighteen-pulse converter will operate at less than 3% ITHD. Three six-pulse converters fed by a phase-shift transformer to provide eighteen-pulse operation, as shown in Fig. 1.4 and 1.5.

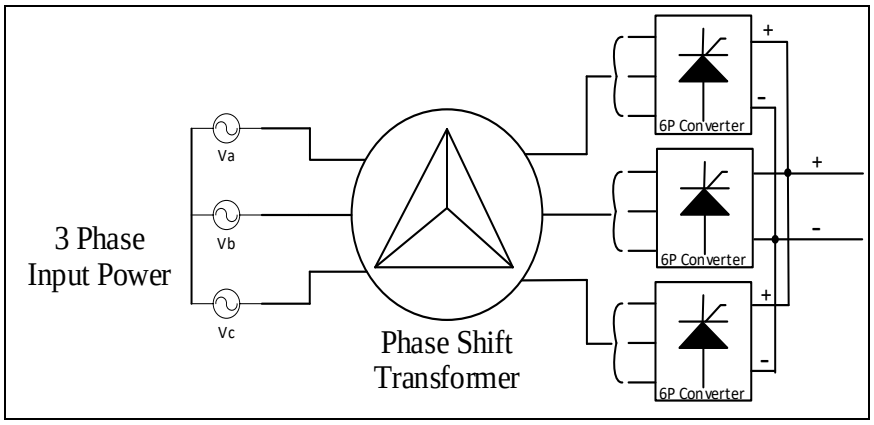

Figure 1.4 Eighteen-Pulse Pulse Converter

Again, care must be taken to understand whether the phase-shifting transformer is included in the VSD or must be supplied separately. Twenty-four and higher pulse numbers can be implemented cost-effectively in higher horsepower systems. Twenty-four pulse converters use phase-shifting transformers to shift each converter by seven degrees and achieve close to 2% ITHD in less background voltage distortion [37].

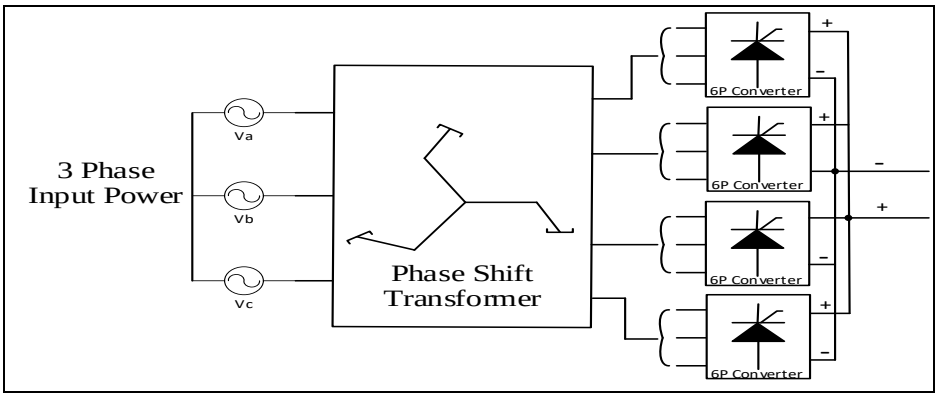

Figure 1.5 Twenty-Four Pulse Converter

Multi-pulse converters can be paired with the appropriate DC bus components and combined with any of the following inverters to make a fully functional VSD.

1.5.4 Current Source Inverters

As stated earlier, the DC bus in a VSD provides either a current or voltage source to an inverter. In a current source inverter, large inductors are used to supply a current source to the inverter. The current supplied to the inverter is normally controlled by an SCR. This is an example of the output inverter type of the VSD influencing the choice of the input rectifier type.

The current source inverter controls only the output frequency of the drive, while the current and voltage are controlled by the input converter. The inverter may operate in either six steps or Pulse Width Modulated (PWM), both to be discussed in the following section. Current source technology is typically the preferred method in extremely high horsepower systems, say $5{,}000^{+}$ HP, due to the availability of the necessary power semiconductor devices at those voltage and current ratings.

1.5.5 Voltage Source Inverters

Large banks of capacitors act as low-impedance DC voltage sources or the inverter in a voltage source inverter. The inverter then changes this DC voltage into AC voltage by one of the various switching methods. These methods generally fall into two categories: Variable Voltage Inverters (VVIs) or Constant Voltage Inverters (CVIs). VVIs usually employ a controlled rectifier, mentioned earlier, to control the DC bus voltage and thereby the output voltage of the inverter. In a CVI, the output voltage is controlled by the method of switching.

1.5.6 Variable Voltage Inverters (Six-Step Inverters)

Variable Voltage Inverters (VVI) drives are most generally six-step inverters. The unit consists of six switches, each one turning on and off one time during every output cycle. The name comes from the fact that each cycle is divided into six 60-degree periods. During each

period, there is a unique combination of power devices activated. This results in a phase-to-phase voltage waveform that has six identifiable "steps" to approximate a sine wave. This is also referred to as a "quasi-sine-wave" inverter. The inverter controls only the output frequency and is a relatively simple and rugged topology. Since the unique characteristics of the six-step waveform the electrical stresses on the power devices are significantly reduced over other topologies.

1.5.7 Pulse Width Modulated Inverters

Pulse Width Modulated (PWM) inverters also consist of six switches, but they switch many times per output cycle to control both output voltage and frequency. For this reason, they are typically fed by an uncontrolled diode bridge rectifier. In a PWM inverter, the voltage waveform is divided into many small periods. The number of periods can range from a few hundred to several thousand. During each period, the instantaneous output voltage is approximated by a square wave at some duty cycle. A 100% duty cycle would represent full voltage, and a 0% duty cycle would represent zero voltage.

To generate a sine wave, these "pulses" would start at zero width and build, sinusoidally, to a 100% duty cycle at the 90-degree point of the waveform. Then they would decrease in width sinusoidally to zero again at a 180-degree point of the waveform. The connections to the motor would then be reversed, and the process would repeat to finish the waveform. The output voltage level is the integral of these pulse widths of DC bus voltage height over any given cycle. This integration is performed by the inductance of the motor, and the resultant current waveform becomes more and more sinusoidal as more pulses are used. To vary the average voltage, each

pulse width is multiplied by a scale factor. To get half the output voltage, each pulse would be one-half of its original width.

The electrical stresses on the power devices of a PWM inverter are significantly higher than on a six-step inverter. Each switching transition causes high losses in the power devices, occurring hundreds or thousands of times per cycle. Because of this, greater care must be taken to ensure that the losses and the resulting voltage stresses are managed properly. This can add to the complexity and cost of this type of inverter. PWM inverters are also used in some current source topologies. In this configuration, the PWM inverter may be combined with an SCR to regulate the current source.

1.6 PMSM Machine Controller Methods

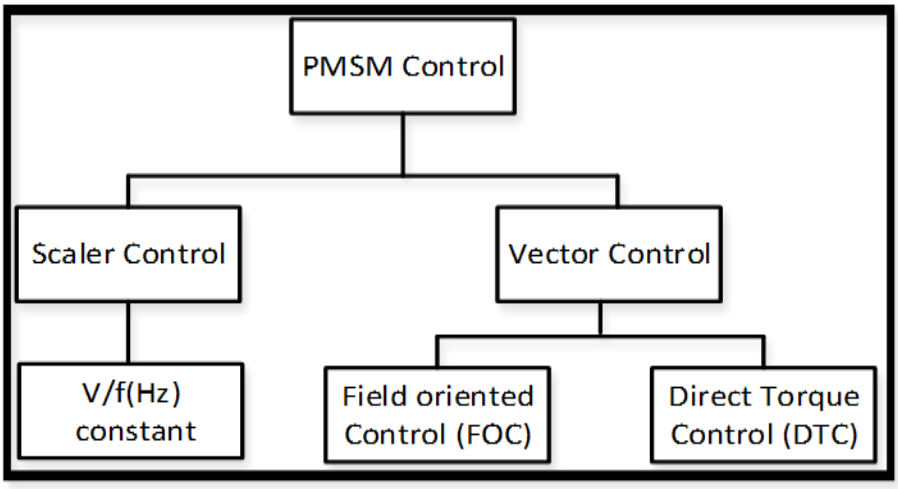

Figure 1.6 PMSM Control Schemes

1.6.1 V/Hz Control Method

V/Hz control is one of the simplest control techniques, where the speed of the PMSM can be controlled by varying the supply frequency [38]. The use of V/Hz control first started for Induction Motor (IM) which does not require a very fast dynamic response. Various techniques were reported for the improvement of V/Hz-control-based IM drive performance [39], [40]. However, the open-loop V/Hz control of wound-field synchronous motor without damper winding is inherently unstable beyond a certain frequency range [41],[42]. The stabilization can be done by providing for the effect of damping torque using an appropriate control strategy during speed transients of the rotor. The methods of stabilizing a synchronous motor using a speed sensor are reported [43]. An additional speed or position sensor, as used in most cases, impose increases the cost and reduces the system's reliability. Rotor position estimation using stator voltage and current has also been reported in the literature. Different stabilization techniques with proper power factor control using DC-link current sensing and DC-link peak current control [44].

1.6.2 Field-Oriented Control (FOC)

The field-oriented control is one of the most efficient techniques used to control the Permanent Magnet Synchronous Motor (PMSM). The high-level efficiency comes at the expense of complex control algorithms that require the angular position of the rotor during the operation. The angular position of the rotor is obtained by a position sensor such as an encoder, a resolver, or a hall sensor [45]. Although Field Oriented Control can be robust using the hall sensor, however, the cost and reliability of the sensor approach are of more concern. For that reason, a sensor-less implementation of the FOC is a step towards a reduction in the costs of drives

comprised of PMSMs and an improvement in their reliability. While the position sensor for some reason may stop working, sensor-less algorithms work if the motor itself together with the power electronics is operational. Sensor-less observers of the angular position and speed of the rotor can be based on the voltage or the current model of the motor. They can be implemented either in the stator reference frame or in the rotor reference frame, although the combination of variables from both reference frames, as presented in [46], is also feasible.

1.6.3 Direct Torque Control

Direct Torque Control (DTC) for induction machines started in the middle of the 1980s, more than four decades ago. It is getting more and more popular nowadays [47]. The basic idea of DTC for induction motor stators is to control the torque and flux linkage by selecting the voltage space vectors properly, which is based on the relationship between the slip frequency and the torque. In the late 1990s, DTC techniques for Permanent Magnet Synchronous Machine (PMSM) machines appeared [48]. The DTC technique is different from the conventional vector control method, where torque is controlled in the rotor reference frame via current control loops [49]. The DTC achieves high torque performance under transient and steady-state conditions. DTC technique uses electromagnetic torque and flux as the control variable, where the feedback signal is obtained through flux and torque estimator [50]. Sliding mode control-based speed control of PMSM drive is presented in [51],[52], which improves the performance of the drive under parameter uncertainty and load disturbance, however, it suffers from the chattering phenomenon.

1.7 Research Contributions

The notion of implementing modeling and analysis of the ESP system to improve the controllability and reliability of SPM is relatively recent. Several open research questions about the controllability and reliability of PMM for ESP system applications have been asked. This dissertation presents a mathematical model and simulation of SPM control that can be used to obtain answers that would impact the reliability, performance, and power quality of the system. The modeling, simulation, and experiment results of the novel sensor-less Modified DTC-SVM SPM-control for ESP system is the main contribution of the dissertation which address the following

1. Improved System Reliability and Reduced System Cost

Develop and model modified sensor-less direct torque control with constant switching frequency and low torque ripple to control SPM for ESP system. The sensor-less control systems should be robust to operating conditions, both steady-state and transient (fast varying load) conditions. In addition, the sensor-less control should be reliable and robust to the variations of machine parameters

2. Increase System Efficiency

Develop Mathematical and Simulation models of the ESP system with proposed control to improve system efficiency. The analytical model includes a sine wave filter, step-up transformer, three-phase cable, pump, and SPM. The final part of the research is to use the analytical model for the optimization of the system. The optimization consists of two parts maximizing system efficiency and minimizing the losses in the machines.

1.8 Research Objectives

The overall objective of this dissertation is to present novel control strategies for the design, analysis, modeling, and implementation of sensor-less a Modified DTC-SVM SPM-drive for ESP systems.

1. Develop a mathematical model using MATLAB /Simulink of a modified DTC-SVM SPMSM controller of the ESP system. The strategy is to focus on the design for optimal error between the estimated and actual values.
2. Implement the proposed control to derive the ESP system.
3. Evaluate the stability of the system under different operating conditions.
4. Evaluate performance data under different operational conditions to measure the motor performance curves and perform a complete system analysis
5. System Efficiency improvement

1.9 Outline of Dissertation

The dissertation is organized as follows.

Chapter 1 reviews Electrical Submersible Pumps (ESPs) system and the state-of-the-art for integrated ESP components and discusses the machine selection, power converter topology, and advanced control schemes.

Chapter 2 focuses on review a mathematical analysis and the modeling of a classical DTC for PMSM. Review the advantage and drawbacks of the classical DTC for ESP systems. MATLAB and Simulink are demonstrated.

Chapter 3 present sensor-less Modified Direct Torque Control based on SVM PMSM control for ESP application. Two PIs based controls are used to control torque and flux which

replace the hysteresis comparators in the classic direct torque control. The reference voltage vectors are generated by an SVM unit, exchanges of the switching table. Propose Modified DTC-SVM technique have several advantages such as constant switching frequency and reduced torque ripple.

Chapter 4 shows the mathematical analysis and modeling of an ESP system using DTC-SVM control. The proposed modified direct torque control based on SVM is used to run the SPM machine. The power quality and efficiency of the proposed inverter were evaluated. The performance of the system is verified in the simulation and experimentally.

Chapter 5 investigates the efficiency improvement, power quality, and system performance of an ESP system. The modeling and experimental results show the efficiency of the system is improved with the analytical model of the system.

Chapter 6 concludes the dissertation and presents suggestions for future research.

Chapter 2: Review and Analysis of Classical DTC Scheme for PMSM

2.1 Introduction

As stated in Chapter 1, classical Direct Torque Control (DTC) for induction motors was first introduced in 1980' [53]. The DTC technique is different from the traditional vector control method, where torque is controlled in the rotor reference frame via a current control loop. classical DTC is a very simple control scheme where no complicated coordinate transformations and decoupling calculations are required [54]. A switching table is implemented to select proper voltage space vectors to apply directly to the motor according to electromagnetic torque errors and the position of the stator flux vector. DTC is lower parameter dependence, where only stator resistance and inductance parameters are required. In addition, no mechanical speed or position sensor is required. These make the system more robust and easier to implement.

DTC techniques for Permanent Magnet Synchronous Machines (PMSM) appeared in 1990 [55]. Great effort has been made in the development of senseless control schemes; an initial rotor position estimation strategy is presented for a DTC PMSM drive. The DTC's faster torque response and robustness to various speed and load conditions attracted research attention in both academia and industry [56].

This chapter, reviews, and analysis the classical DTC scheme for PMSM. Section 2.2 presents mathematical models of PMSM. Followed by the design and analysis of the classical DTC scheme for PMSM in section 2.3. Section 2.4 incorporates modeling and analysis sensors in classical DTC PM machines.

2.2 Mathematical Model and Analysis of SPM

Based on assumptions that saliency, saturation, and iron losses are negligible, the mathematical modeling of the SPM machine in the synchronous rotor (*d-q)* reference frame voltage and torque, the SPM machine can be described by the following equations [57].

$$v_{ds} = \mathrm{R_s} i_{ds} + \mathrm{L_s} \frac{d i_{\alpha s}}{dt} - \mathrm{L}_s \omega_r i_{qs} \quad 2.1$$

$$v_{qs} = R_s i_{qs} + L_s \frac{d}{dt} i_{qs} - L_s \omega_r i_{ds} + \omega_r \psi_m \quad 2.2$$

$$\psi_{ds} = L_s i_{ds} + \psi_m \quad 2.3$$

$$\psi_{qs} = L_s i_{qs} \quad 2.4$$

$$T_e = \frac{3}{2} \mathrm{P} \left(\psi_{ds} i_{qs} - \psi_{qs} i_{ds} \right) = \frac{3}{2} \mathrm{P}\, \psi_m i_{qs} \quad 2.5$$

For SPM the reluctance torque is zero since $L_d = L_q$, where V_{ds}, V_{qs}, i_{ds} and i_{qs} are the direct and quadrature axis of voltage and current respectively. The stator winding resistance and inductance are R_s and L_s. ψ_m is the permanent magnet flux linkage, a machine with P pole pairs.

The stationary reference frame voltage can be expressed as:

$$v_{\alpha s} = R_\alpha i_{\alpha s} + L_s \frac{d i_{\alpha s}}{dt} - \omega \psi_m Sin(\theta) \quad 2.6$$

$$v_{\beta s} = R_s i_{\beta s} + L_s \frac{d i_{\beta s}}{dt} - \omega \psi_m Cos(\theta) \quad 2.7$$

$$\psi_{\alpha s} = L_s i_{\alpha s} + \psi_m Cos(\theta) \quad 2.8$$

$$\psi_{\beta s} = L_s i_{\beta s} + \psi_m Sin(\theta) \quad 2.9$$

The rotor angle can be found by the following equation.

$$\Theta_r = \tan^{-1}(\psi_{m\beta} / \psi_{m\alpha}) \quad 2.10$$

The real and imaginary components of the stator voltage and current space vectors are $V_{s\alpha}$, $V_{s\beta}$, $i_{s\alpha}$ and $i_{s\beta}$ [58]. The rotor speed and angular position are given respectively ω and θ.

2.3 Review and Analysis of Classical DTC Scheme for PMSM

DTC-SVM drive functional block diagram shown in Fig. 2.1 has been implemented experimentally. A standard DTC algorithm based on the selection of an output voltage vector, the electromagnetic torque, and stator flux is used. There are three comparators in the DTC block. The first hysteresis comparator is torque control flags which determine the increase or decrease of the torque. The second hysteresis comparator is flux linkage controllers compare the estimated electromagnetic torque and stator flux linkage with their respective reference values [59]. DTC uses no current controller and motor parameters other than the stator resistance and inductance used for flux estimation, which yields a faster torque response and lower parameter dependence. Flux control flag which controls flux magnitude. The third comparator is the sector generator that detects in which sector of the circle the flux vector exists. The stator flux reference (ψ^*) value is compared with the estimated stator flux ($\hat{\psi}$) value. Reference electromagnetic torque (T^*) is compared with the estimated electromagnetic torque ($\hat{T}$). Flux $\Delta\psi$ and torque ΔT error are input to the flux and torque comparators respectively. The outputs of torque and flux comparator (δT and $\delta\psi$) are sent to the inverter switching table for proper selection of voltage control in the Voltage Source Inverter (VSI)

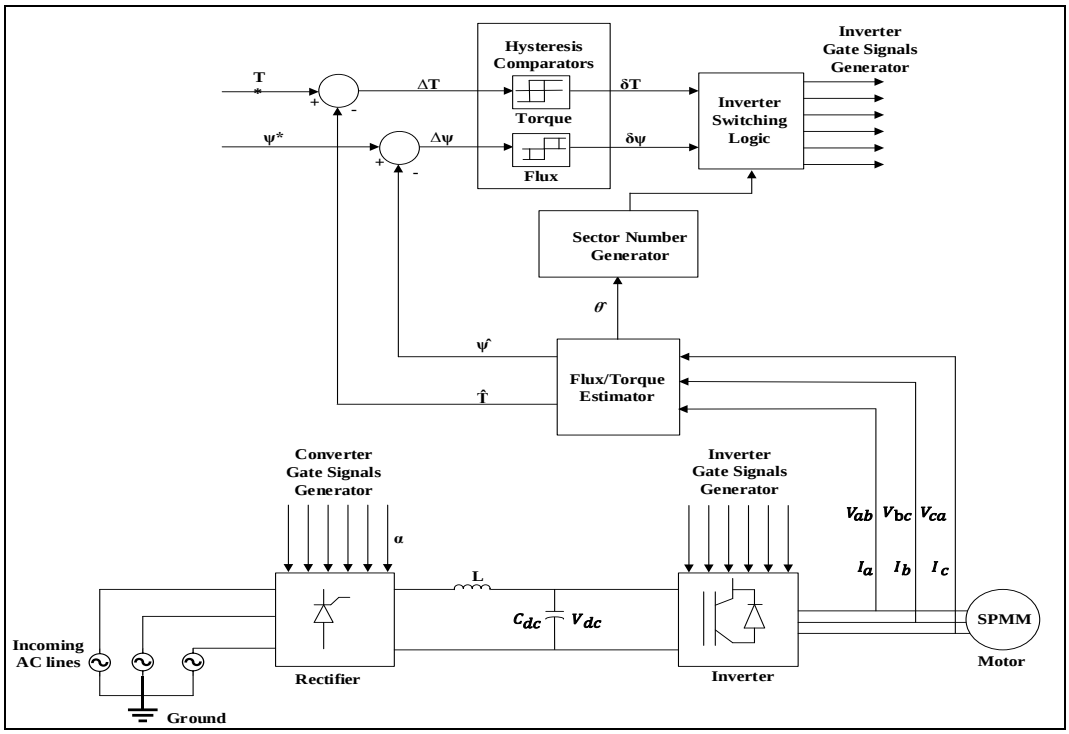

Figure 2.1 Direct Torque Control (DTC) Scheme for SPM

According to Table 2.1, The controllers select the optimal voltage vector for all the possible stator flux space vector positions and determine the control input. A Voltage Source Inverter (VSI) controller is used to supply voltage to the PMSM, the electromagnetic torque and the stator flux are directly controlled by selecting the optimum stator voltage space vector, and the errors in the torque and flux controllers directly feed to the inverter without any intermediate current control loop [60], as shown in Fig. 2.2. It is important to keep torque and flux controllers as hysteresis types to improve dynamic control. The outputs are used to determine which of the possible inverter states should be applied to the motor terminals so that the errors in the flux and torque remain within the prescribed hysteresis band (H^{ψ}).

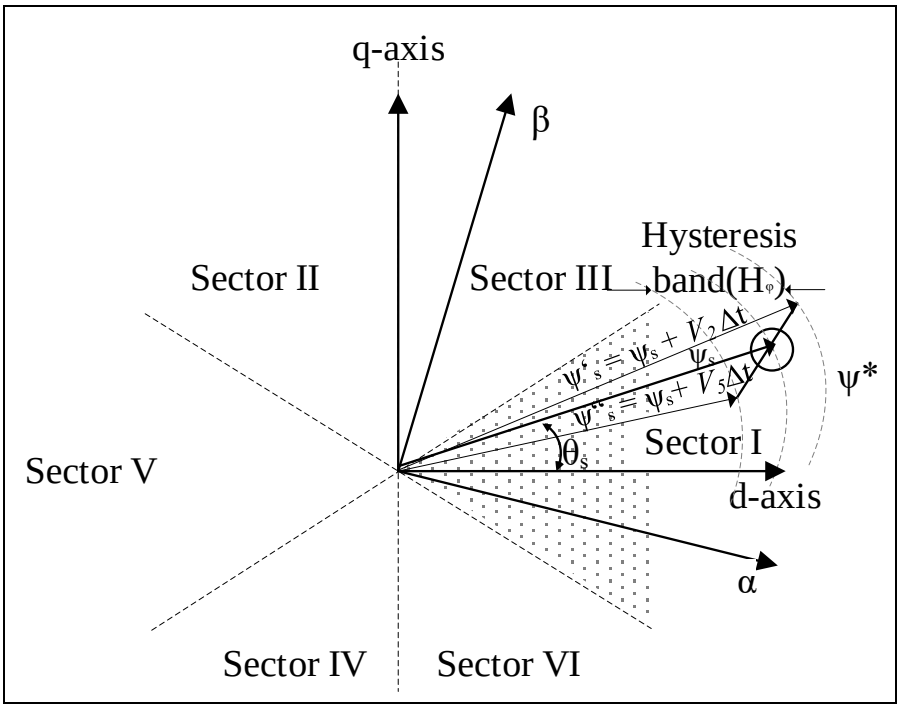

Figure 2.2 Stator Flux Phasor Diagram in dq and $\alpha\beta$.

The flux controller is a two-level hysteresis comparator while the torque controller is a three-level hysteresis comparator. The digitized output signals of the flux controller are defined as those of the torque controller

$$\delta\psi = +1 \quad \text{if } |\hat{\psi}| \leq |\psi*| - |H^{\psi}| \tag{2.11}$$

$$\delta\psi = 0 \quad \text{if } |\hat{\psi}| \geq |\psi^*| + |H^{\psi}| \tag{2.12}$$

$$\delta T = +1 \quad \text{if } |\hat{T}| \leq |T^*| - |H^{\psi}| \tag{2.13}$$

$$\delta T = 0 \quad \text{if } |\hat{T}| = |T^*| \tag{2.14}$$

$$\delta T = -1 \quad \text{if } |\hat{T}| \geq |T^*| + |H^{\psi}| \tag{2.15}$$

The Inverter switching table can be derived by using physical considerations since the voltage space vector affects the development of the torque at each switching instant. Assume

that ψ*is in the sector I, the comparator output $\delta T = \delta\psi = +1$, if $\hat{T}$ and $\hat{\psi}$ are increased significantly then voltage vector V_2 can be selected from equation 2.1.

Table 2.1 Inverter Switching Table [61]

δψ	δT	Sector I	Sector II	Sector III	Sector IV	Sector V	Sector VI
1	1	V_2	V_3	V_4	V_5	V_6	V_1
	0	V_7	V_0	V_7	V_0	V_7	V_0
	-1	V_6	V_1	V_2	V_3	V_4	V_5
0	1	V_3	V_4	V_5	V_6	V_1	V_2
	0	V_0	V_7	V_0	V_7	V_0	V_7
	-1	V_5	V_6	V_1	V_2	V_3	V_4

The inverter switching table above shows δψ and δT are the outputs of the flux and torque hysteresis controllers respectively. $\Delta\psi = 1$ implies that the estimated flux is smaller than its reference value and $\Delta\psi = 0$ reference flux is greater. The δT compares estimated and reference torque, the sectors provide the approximate position information of the stator flux linkage with of 60° electrical angle in the stationary reference frame.

2.4 Simulation Results

The MATLAB/Simulink modeling for DTC-SVM of SPM is developed based on the scheme presented in Fig. 2.3. The SPM motor parameters used in the simulation are listed in the table below.

Table 2.2 Parameters of the SPM Machine

Rated Output Horsepower (Hp)	250
Rated Voltage (Volt)	2575
Rated Current (A)	50
Rated Speed (RPM)	3600
Rated Torque (Nm)	494.5
Poles	4
Stator resistance Rs (Ω)	1.052
Stator inductance L_d=L_q (mH)	20

2.4.1 Starting Mode

During starting the actual electromagnetic torque (T*) is compared with the estimated electromagnetic torque. The actual torque tracks estimated torque as shown in Fig. 2.3 (i). The PM machine accelerates from 0 to 3600 rpm. After the machine reached its rated speed of 3600 rpm, generates a rated torque of 494.49 Nm. The stator current waveform under the starting condition is shown in Fig. 2.3 (iii) it reaches the rated value at full load. However, the current waveform has experienced a lot of distortion because of the torque ripples generates by the Hysteresis comparator.

As shown, the DC bus voltage is controlled under 650 V, and the output frequency tracks the estimated frequency and reached the maximum value (120 Hz). When the DC bus reaches the required value as shown in Fig. 2.4.

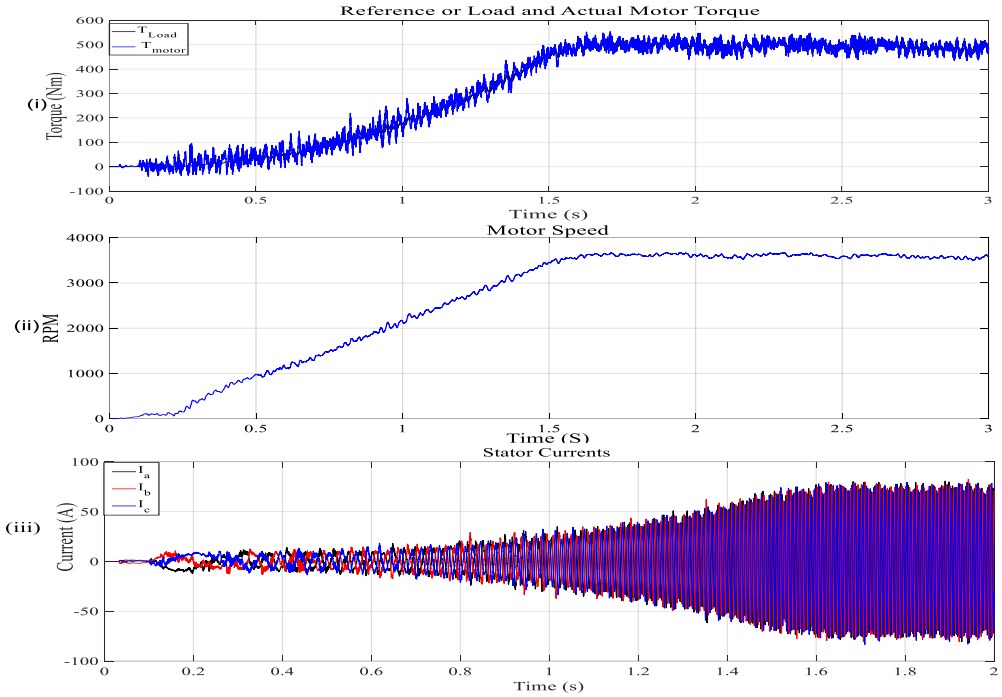

Figure 2.3 DTC Motor Electromagnetic Torque, Motor Speed, and Stator Current Starting Process

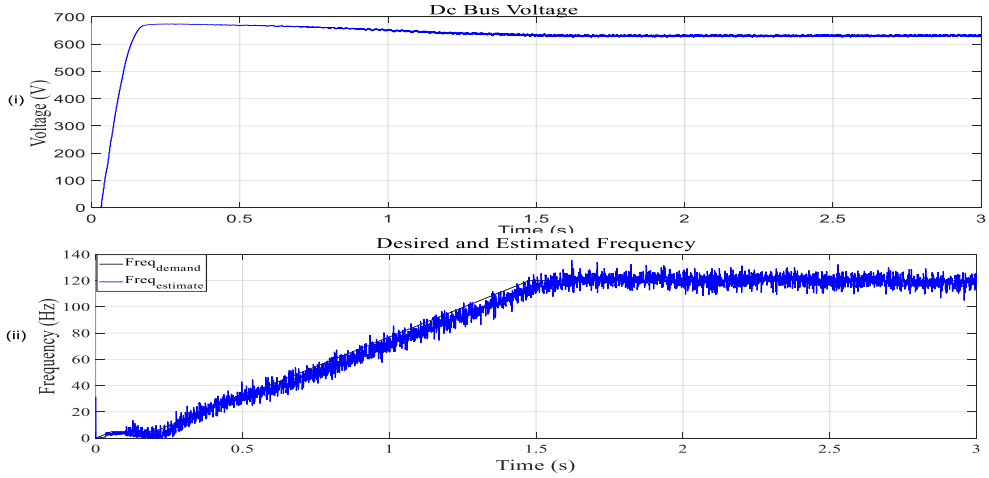

Figure 2.4 DTC Starting DC Bus Voltage and Controller Output

2.4.2 Steady State Mode

The Steady-state performance torque, speed, controller output frequency, and stator current when the PM machine runs at 3600 rpm with a full load are shown in Fig. 2.5. The torque and the controller output frequency fluctuate are 30 Nm and 5 Hz respectively. Torque ripples are highly generated undesirable noise and cause extra losses in the stators. The stator current waveform under this condition generates high current distortion. Fig. 2.6 shown DTC DC Bus and Controller Output Frequency at 60 Hz.

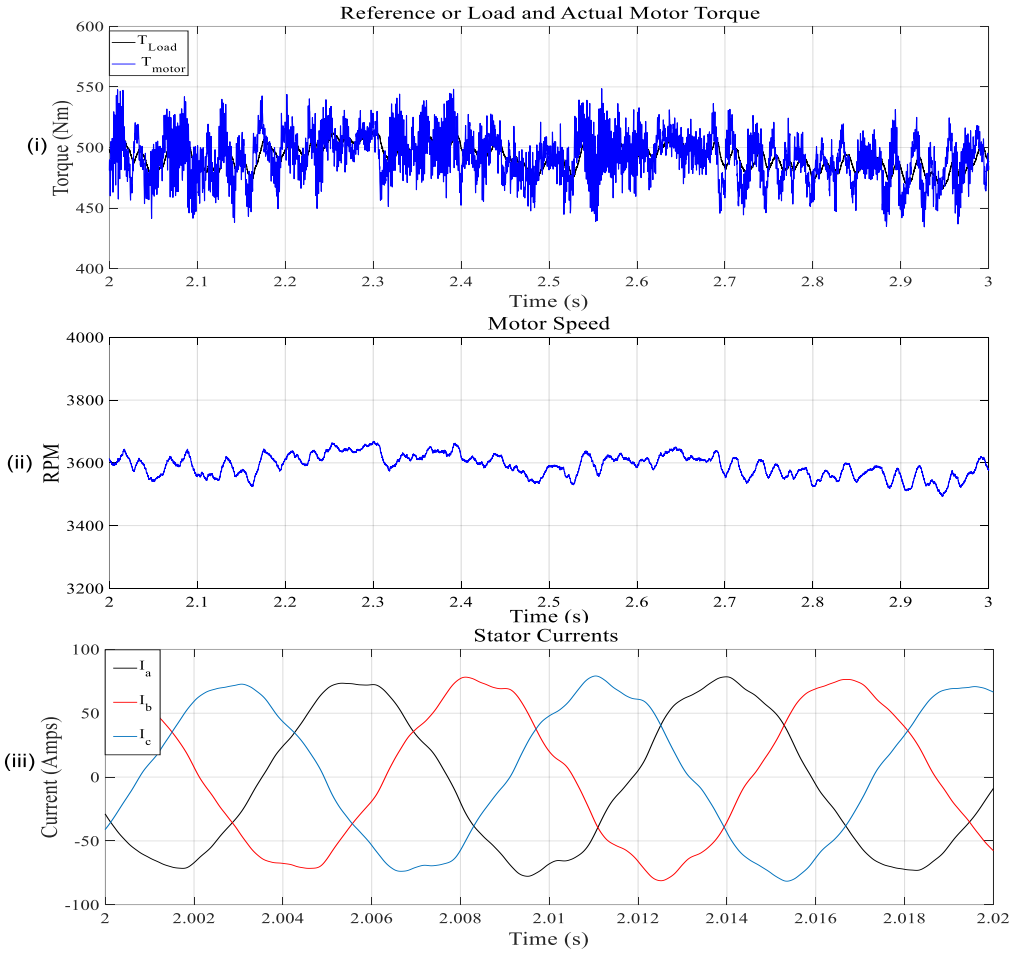

Figure 2.5 DTC Motor Torque, Motor Speed, and Stator Current with Full Load at 3600 rpm

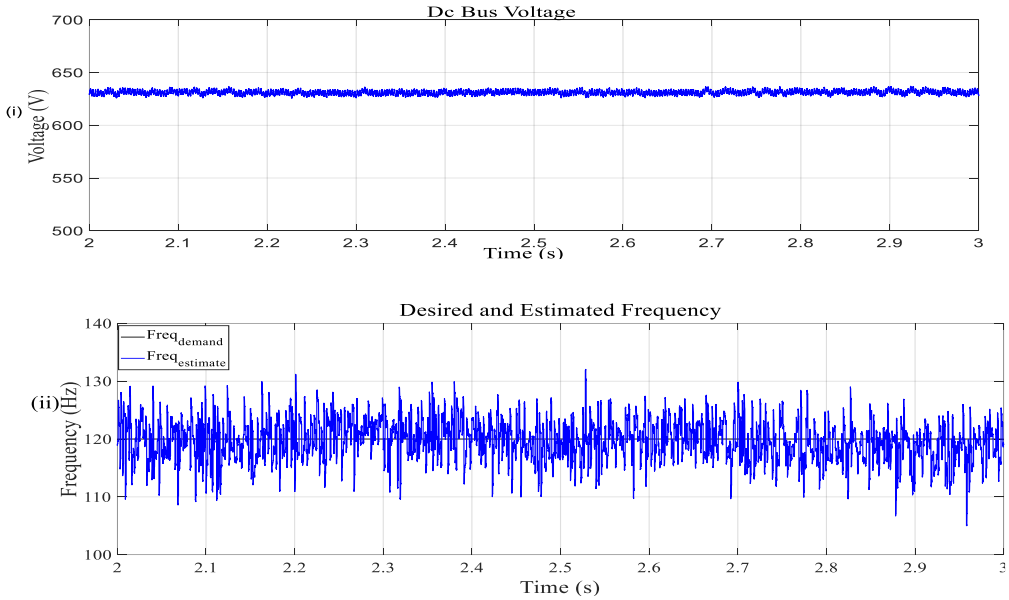

Figure 2.6 DTC DC Bus and Controller Output Frequency at 60 Hz.

2.5 Conclusion

The direct torque-controlled PM machine for ESP application has been analyzed and verified with MATLAB/Simulink simulation. The results show that the direct torque control concept had been successfully prolonged to control the SPM machine. Although the torque ripples and current distortion are rather large, the machine runs full load at the rated speed. The drawback of the hysteresis-based DTC schemes is variable switching frequency and current and torque distortion caused by the sector generator [62].

Modified Sensor-less DTC schemes with space vector modulation are presented in the next chapter. The DTC strategies operating at constant switching frequency can be implemented using PI-controlled closed-loop schemes. The controllers calculate the required stator voltage

vector over a sampling period. The voltage vector is synthesized by a PWM technique, which in most cases is the Space-vector Modulation (SVM).

Chapter 3: Modeling and Analysis of Modified Sensor-less Direct Torque Control with Space Vector Modulation (SVM)

3.1 Introduction

In the previous chapter the Direct Torque Control (DTC) scheme has been studied and implemented on the SPM motor drive. Also, the advantages of the system are stated; the common disadvantages of the hysteresis-based DTC schemes are variable switching frequency, high torque and current ripples caused by sector generator, and difficulty to estimate torque and flux at very low speeds [63]. Several modified DTC schemes based on Space Vector Modulation (SVM) researchers have attempted to overcome these drawbacks [64]. However, this scheme generates noise due to the differentiation term in the feed-forward path [65]. This chapter proposes a direct torque and flux control scheme for SPM. In effect, flux and torque hysteresis comparators are replaced by two Proportional-Integral (PI) controllers. Constant switching frequency and lower torque ripple are achieved with the PI controller and Space Vector Modulation (SVM). The desired voltage vectors at a constant switching frequency are generated by an SVM unit, which replaces the switching table in the classical DTC scheme [66]. Whilst retaining the main advantage of classic DT, the proposed modified DTC-SVM technique offers:

- Constant switching frequency,
- Reduced torque ripple,
- Better DC bus utilization,
- Lower current Total Harmonic Distortion (THD), and lower switching losses.

This chapter is organized as follows, Section 4.2 Presents a detailed analysis of the principle for direct torque and flux control-based SPM systems. Followed by space vector modulation analysis. Finally, the simulation and experimental results in section 3.3.

3.2 The Direct Torque and Flux Control (DTFC) Scheme for the SPM Machine

A similar scheme DTFC for PM motor drives application has been presented in [67]. However, its application in ESP motors or the ESP system has not been reported. Also, Sensor-less direct torque and flux controlled IPM synchronous motor drives are studied in detail [68]. The SVM-DTFC controller consists of flux and torque PI controllers as indicated in Fig. 3.1 below.

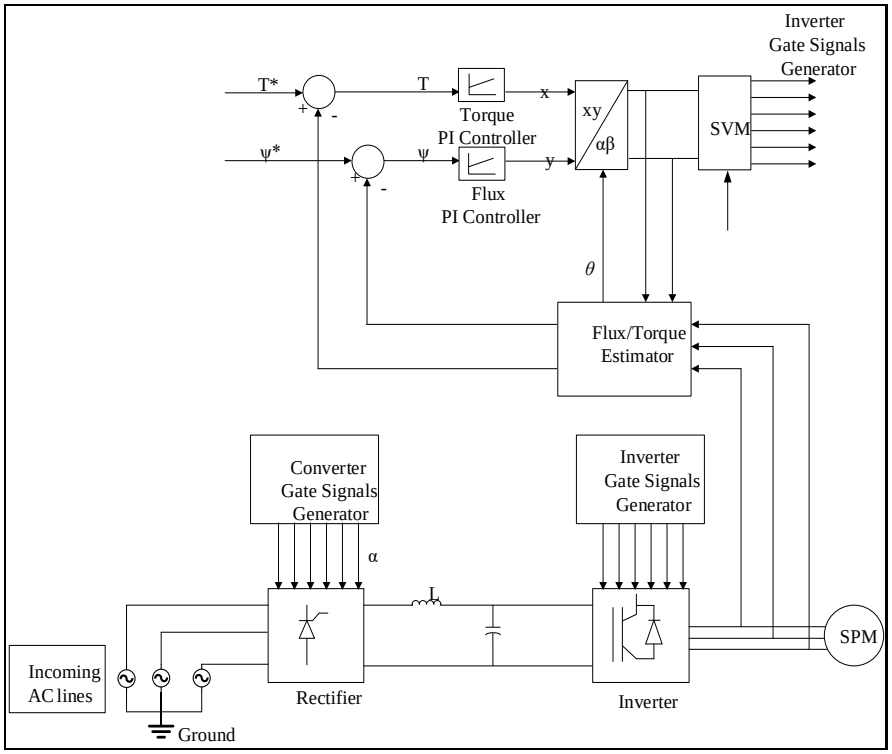

Figure 3.1 Schematic Diagram Modified DTC-SVM with Closed-Loop Torque Control

The reference and estimated torque and flux errors are used as inputs to the torque and flux PI controllers respectively. The output of the PI controllers generates the *x-y* reference

voltage vector (V_x^* and V_y^*) which can be transformed into the stationary (α-*β)* reference frame to generate the SVM for the inverter. If the torque and flux errors are too large during transients, the reference voltage may be larger than the existing inverter voltage [69]. In this state, the outputs of the PI controllers must be limited to the reference voltage (V_{ref}) being less or equal to the maximum inverter voltage (V_{max}).

$$(V_{ref}) \leq (V_{max}) \tag{3.1}$$

Under modulation of SVM,

$$V_{max} = \frac{V_{DC}}{\sqrt{3}}, \tag{3.2}$$

where V_{DC} is the DC bus voltage of the inverter

$$V^*(x, y) \leq \frac{V_{DC}}{\sqrt{3}} \tag{3.3}$$

Voltage transform into the stationary reference frame

$$\begin{bmatrix} V_\alpha \\ V_\beta \end{bmatrix} = \begin{bmatrix} cos\,\theta & -sin\,\theta \\ sin\,\theta & cos\,\theta \end{bmatrix} \begin{bmatrix} V_x \\ V_y \end{bmatrix} \tag{3.4}$$

where θ' is the stator flux angle and it can be calculated

$$\theta = \tan^{-1} \frac{\psi_\beta}{\psi_\alpha} \tag{3.5}$$

From equations 3.1 and 3.2 can be represented in the stator reference frame as [70].

$$v_x = R_s i_x + \frac{d\psi_x}{dt} - \omega_s \psi_y \tag{3.6}$$

$$v_y = R_s i_y + \frac{d\psi_y}{dt} - \omega_s \psi_x \tag{3.7}$$

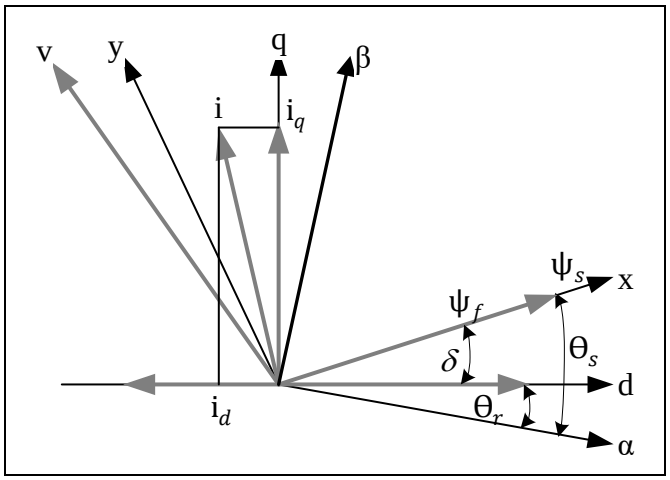

Figure 3.2 The Stator and Rotor Flux Linkages in Various Reference Frames.

where, ω_s is the speed of the stator flux vector. From Fig. 3.2 the stator flux vector is aligned with the x-axis, therefore:

$$\psi_x = |\psi_s| \text{ and } \psi_y = 0 \tag{3.8}$$

$$\psi_q = \psi_s \sin\delta \text{ and } \psi_d = \psi_s \cos\delta \tag{3.9}$$

Therefore substituting 3.18 into 3.16 and 3.17

$$v_x = R_s i_x + \frac{d\psi_s}{dt} \tag{3.10}$$

$$v_y = R_s i_y - \omega_s \psi_s \tag{3.11}$$

The stator electromagnetic torque and flux linkage in the αβ stationary reference frame can be estimated.

$$T_e = \frac{3}{2}P\left(\psi_\alpha i_\beta - \psi_\beta i_\alpha\right) \tag{3.12}$$

$$T_e = \frac{3}{2}P\left(\psi_\alpha i_\beta - \psi_\beta i_\alpha\right) \tag{3.13}$$

where: $\psi_\alpha = \int(v_\alpha - R_s i_\alpha)dt$ and $\psi_\beta = \int(v_\beta - R_s i_\beta)dt$ 3.14

$$\psi = \sqrt{{\psi_\alpha}^2 + {\psi_\beta}^2} \quad 3.15$$

The SVM algorithm is used to synthesize the desired voltage vectors at a constant switching frequency.

3.2.1 Design of PI Controller

In the SVM-DTFC controller system, the steady-state and dynamic responses are mainly affected by the PI controller parameters. PI controller is a type of feedback controller that has output depending upon the error. If the torque and stator flux responses error are too large, the controller may be unstable. This error is used to adjust the input of the other process. Two parameters are used to design this controller. These parameters are the proportional gain (Kp) and the integral gain (K_i). This controller can be represented as

$$G_{PI}(s) = \frac{K_p S + k_i}{S^2} \quad 3.16$$

3.2.2 Torque PI Controller Design

The transfer function torque transfer function block diagram shown in Fig. 3.3 a PI controller is given in equations (3.16), PI transfer function of the close loop torque controller is expressed as:

$$G_{TPI}(S) = \frac{K_{pT} S + K_{iT}}{S} \quad 3.17$$

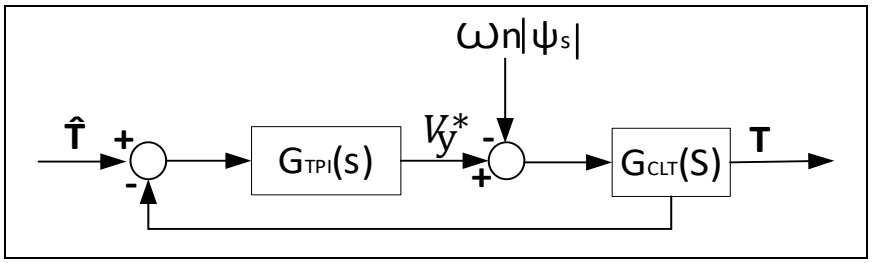

Figure 3.3 Block Diagram of Torque Loop Model.

Block diagram the rotor speed and the stator flux magnitude added to the torque PI.

$$G_{ClT}\ (s)\ =\ \frac{3P\psi_{\ s}\,k\ (T)}{2R_s\ k(T)\ +3SP\psi_s^2 S^2} \tag{3.18}$$

From the function Laplace transfer

$$G_T\ (\mathrm{s})\ =\ \frac{Gp_T\ (\mathrm{S})\ G_{PIT}\ (\mathrm{S})}{1+G_{PT}\ (\mathrm{S})\ G_{PIT}\ (\mathrm{S})} \tag{3.19}$$

$$=\ \frac{3P\,\psi_s\ \mathrm{k}\ (\mathrm{T})k_{PT}\,\mathrm{S}\ +\ 3P\psi_s\ \mathrm{k}\ (\mathrm{T})\ k_{iT}}{3P{\psi_s}^2S^2\ +\ 2R_s\ \mathrm{k}\ (\mathrm{T})\ +\ 3P\psi_s\ \mathrm{k}\ (\mathrm{T})\ k_{PT}\ +\ 3P\psi_s\ \mathrm{k}\ (\mathrm{T})\ k_{iT}} \tag{3.20}$$

The proportionality and integral coefficients of the torque loop controller with the damping coefficient (ζ) and natural angular frequency ($\mathrm{C}\mathcal{O}n$) of the second order equation the controller gains can be expressed as follows.

$$k_{PT}\ (s)\ =\ \frac{6P\psi\,\zeta_s{}^2\,S^2\ +\ 2R_s\ k\ (T)}{1+G_{PT}\ (S)\ G_{PIT}\ (S)} \tag{3.21}$$

$$k_{iT}\ (s)\ =\ \frac{\mathrm{C}\mathcal{O}n^2\psi s}{k(T)}\ \ where k(T)\ =\ k(T)\ cos\ \delta \tag{3.22}$$

3.2.3 The Stator Flux PI Controller Design

The close loop stator flux transfer function block diagram shown in Fig. 3.4. The flux PI controller transfer function ($G_{\psi PI}$ (s)) is expressed below.

$$G_{\psi PI}(s) = \frac{k_p\psi\, S + k_i\psi}{S} \quad 3.23$$

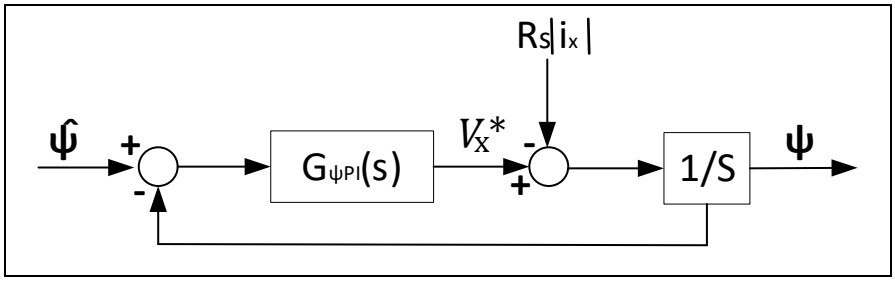

Figure 3.4 Block Diagram of Flux Loop Model.

Note that a decoupling term R_{six} is added to the output of the torque PI regulator to invalidate the effects of the disturbance.

$$G_{\psi}(s) = \frac{\frac{1}{s}.\, G_{\mathbf{PI}\psi}(S)}{1 + \frac{1}{s}.\, G_{\mathbf{PI}\psi}(S)} \quad 3.24$$

$$= \frac{K_{\mathbf{Pi}\psi} + K_{\mathbf{P}\psi} S}{S^2 + K_{\mathbf{i}\psi} + K_{\mathbf{P}\psi} S} \quad 3.25$$

A close loop second-order system transfer equation

$$S^2 + K_{\mathbf{P}\psi} S + K_{\mathbf{i}\psi} \quad 3.26$$

$$S^2 + 2\zeta C\mathcal{O}nS + C\mathcal{O}n^2 = 0 \quad 3.27$$

where the coefficient (ζ) and natural frequency ($C\mathcal{O}n$) close loop second order equation the controller gains can be expressed as follows.

$$K_{\mathbf{i}\psi} = C\mathcal{O}n^2 \quad 3.28$$

$$K_{\mathbf{P}\psi} = 2\zeta C\mathcal{O}n \quad 3.29$$

MATLAB/Simulink software is used to validate the DTFC-SVM and tunes the flex and torque PI. The damping coefficient and natural frequency of the torque and flux loop for SPM

machineries were selected to be ζ = 0.8 and ωn = 377 rad/sec respectively. The back-EMF and the stator flux linkage are 638 V/KRPM and 2.487 wb respectively. Consequently, the carrier frequency of PWM is set to 2 KHz. Inverter sampling time is 500 µs and 175 scaling factors are selected to convert analog to digital signal based on 8 bits Analog to Digital Converter (ADC). The gains of the torque PI controller calculated from (3-20) and (3-31) is KpT = 3.02 and KiT = 2.05 and the gains of the flux PI controller calculated from (3-28) and (3-29) is $Kp\psi$ = 6.64 and $Ki\Psi$ = 4.15 to meet the designated parameter of the damping coefficient and natural frequency. Fig. 3.5 represent steady State current (i) DC bus voltage, (ii) electromagnetic torque (iii) stator flux and (iv) stator current.

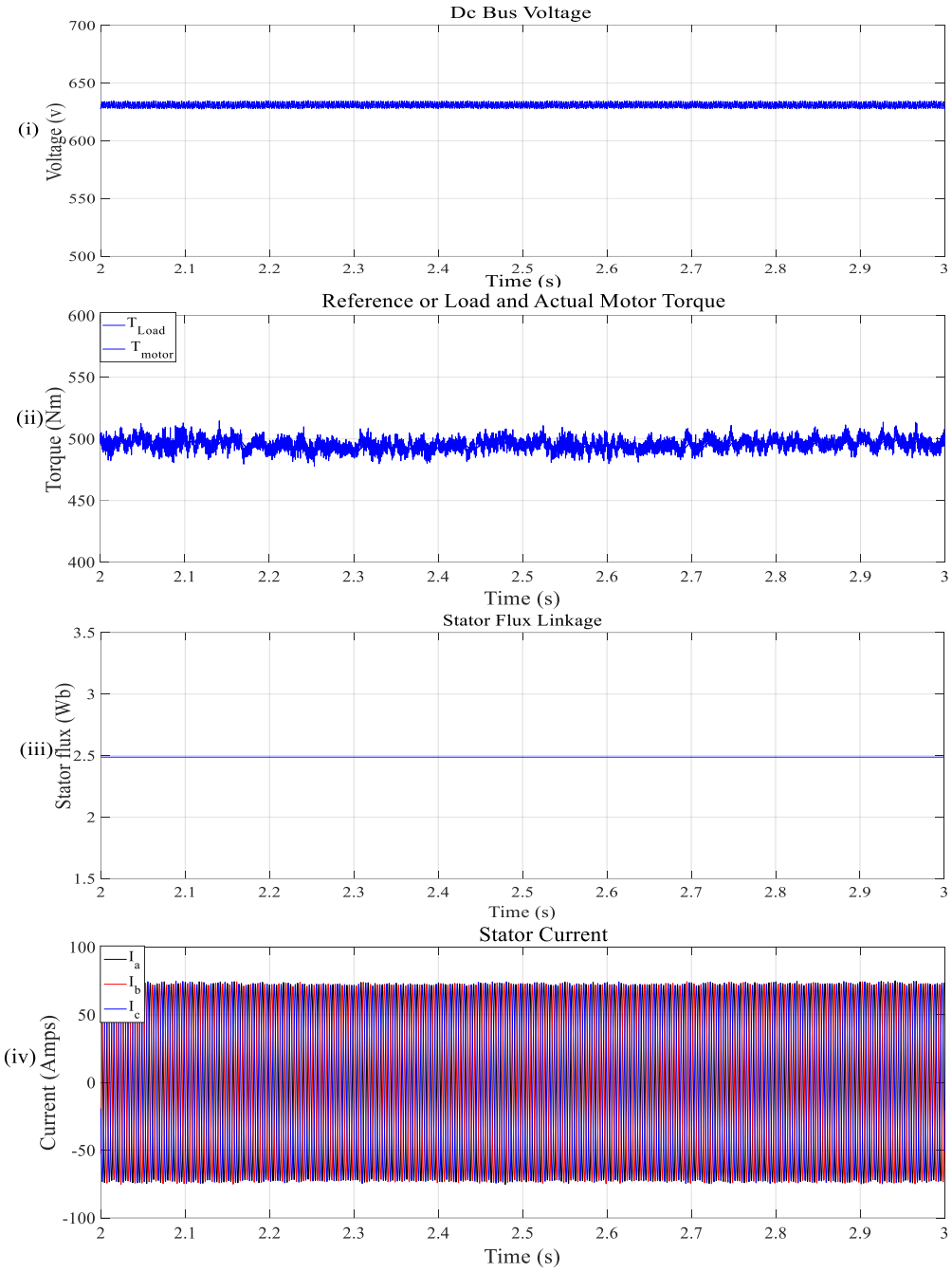

Figure 3.5 DC Bus Voltage, Torque, Stator Flux, and Stator Current with Full Load- Ful Speed Under DTFC

3.2.4 Space Vector Modulation Principle

SVM was presented by a team of German researchers in the middle 1980s. Since then, a lot of research has been done on the theory and implementation of SVM methods. The torque ripple in DTC-SVM is significantly improved, and the switching frequency is maintained constant [71]. The SVM technique transforms voltage components to generate gate signals for the inverter's IGBTs. A three-phase inverter has six IGBTs two per phase positive and negative terminal. The six IGBT in sequence S_1 to S_6 which are controlled by switching variables positive S_1, S_3, and S_s are controlled by (a, b, c), and negative S_2, S_4, and S_6 are controlled by (a', b', and c'). When the positive is gate switched on when switching variables, a, b, and c is 1, the matching negative is gate switched off when switching variables, a', b', and c' is 0. Therefore, the on and off states of positive, gate S_1, S_3, and S_5 can be used to determine the output voltage line-to-line voltage vector (V_{ab}, V_{bc}, V_{ca}), and phase voltage vector (V_a, V_b, V_c) as shown in equation

$$\begin{bmatrix} V_{ab} \\ V_{bc} \\ V_{ca} \end{bmatrix} = V_{DC} \begin{bmatrix} 1 & -1 & 0 \\ 0 & 1 & -1 \\ -1 & 0 & 1 \end{bmatrix} \begin{bmatrix} a \\ b \\ c \end{bmatrix} \quad 3.30$$

$$\begin{bmatrix} V_{an} \\ V_{bn} \\ V_{cn} \end{bmatrix} = \frac{V_{DC}}{3} \begin{bmatrix} 2 & -1 & -1 \\ -1 & 2 & -1 \\ -1 & -1 & 2 \end{bmatrix} \begin{bmatrix} a \\ b \\ c \end{bmatrix} \quad 3.31$$

Based on the equations (3.30 and (3.40), the eight switching vectors, line-to-neutral (phase) voltage, and output line-to-line voltages in terms of DC-link V_{DC}, are given in Table 3.3.

Table 3.1 Switching Vectors, Phase Voltages, and Output Line-to-Line Voltages.

Voltage Vectors	**Switching Variable**			**Line-to-Line Voltage**			**Phase Voltage**		
	a	**b**	**c**	V_{ab}	V_{bc}	V_{ca}	V_{an}	V_{bn}	V_{cn}
V_0	0	0	0	0	0	0	0	0	0
V_1	V_{DC}	0	0	V_{DC}	0	$-V_{DC}$	$2/3V_{DC}$	$-1/3\ V_{DC}$	$-1/3\ V_{DC}$
V_2	V_{DC}	V_{DC}	0	0	V_{DC}	$-V_{DC}$	$1/3V_{DC}$	$1/3V_{DC}$	$-2/3V_{DC}$
V_3	0	V_{DC}	0	$-V_{DC}$	V_{DC}	0	$-1/3V_{DC}$	$2/3V_{DC}$	$-1/3V_{DC}$
V_4	0	V_{DC}	V_{DC}	$-V_{DC}$	0	V_{DC}	$-2/3V_{DC}$	$1/3V_{DC}$	$1/3V_{DC}$
V_5	0	0	V_{DC}	0	$-V_{DC}$	V_{DC}	$-1/3V_{DC}$	$-1/3V_{DC}$	$2/3V_{DC}$
V_6	V_{DC}	0	V_{DC}	V_{DC}	$-V_{DC}$	0	$1/3V_{DC}$	$-2/3V_{DC}$	$1/3V_{DC}$
V_7	V_{DC}	V_{DC}	V_{DC}	0	0	0	0	0	0

The objective of the SVM technique is to approximate the reference voltage vector V_{ref} using the eight switching patterns [72]. One simple method of approximation is to generate the average output of the inverter in a small period, T to be the same as that of V_{ref} in the same period. Six non-zero vectors (V_1 - V_6) and two zero vectors (V_0 and V_7) are conceivable. Six nonzero vectors shape the axes of a hexagonal as depicted in Fig. 3.6, and feed electric power to the load [73].. The angle between any adjacent two non-zero vectors is 60 degrees. Meanwhile, two zero vectors are at the origin and apply zero voltage to the load. The eight vectors are called the basic space vectors and are denoted by V_0, V_1, V_2, V_3, V_4, V_5, V_6, and V_7.

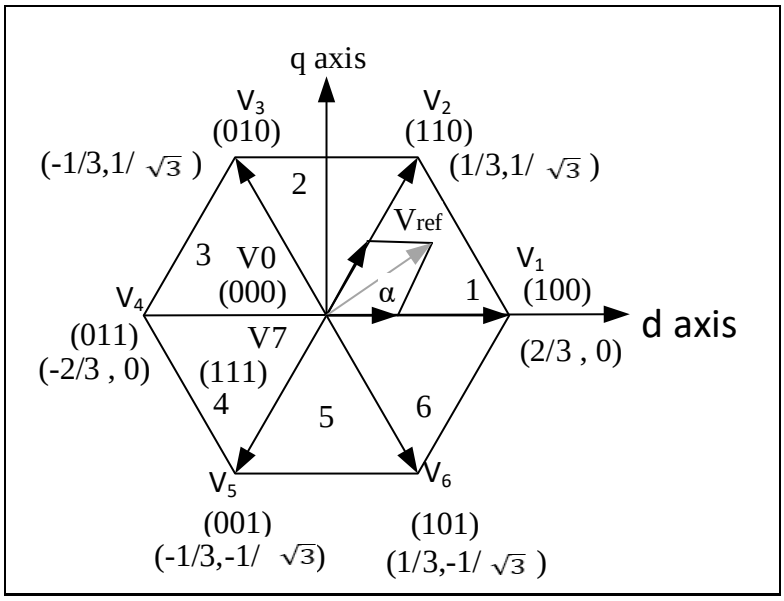

Figure 3.6 SVM Switching Vectors and Sectors.

To implement the space vector, the voltage equations in the *abc* reference frame can be transformed into the stationary *dq* reference frame. From Fig. 3.7, the V_d, V_q, V_{ref}, and angle (α) can be determined as follows:

$$V_d = V_{an} - V_{bn}.\cos 60 - V_{cn}.\cos 60 \quad 3.32$$

$$V_d = V_{an} - 1/2V_{bn} - 1/2V_{cn} \quad 3.33$$

$$V_q = 0 - V_{bn}.\cos 30 - V_{cn}.\cos 30 \quad 3.34$$

$$V_q = V_{an} - \sqrt{3}/2V_{bn} - \sqrt{3}/2V_{cn} \quad 3.35$$

Therefore:

$$\begin{bmatrix} V_d \\ V_q \end{bmatrix} = 2/3 \begin{bmatrix} 1 & -1/2 & 0 \\ 0 & \sqrt{3}/2 & -\sqrt{3}/2 \end{bmatrix} \begin{bmatrix} V_{an} \\ V_{bn} \\ V_{cn} \end{bmatrix} \quad 3.36$$

$$V_{ref} = \sqrt{(V_d)^2 + (V_q)^2} \quad 3.37$$

$$\alpha = tan^{-1}\frac{V_q}{V_d} = \omega t = 2\pi ft \text{ where f is fundamental frequency.} \quad 3.38$$

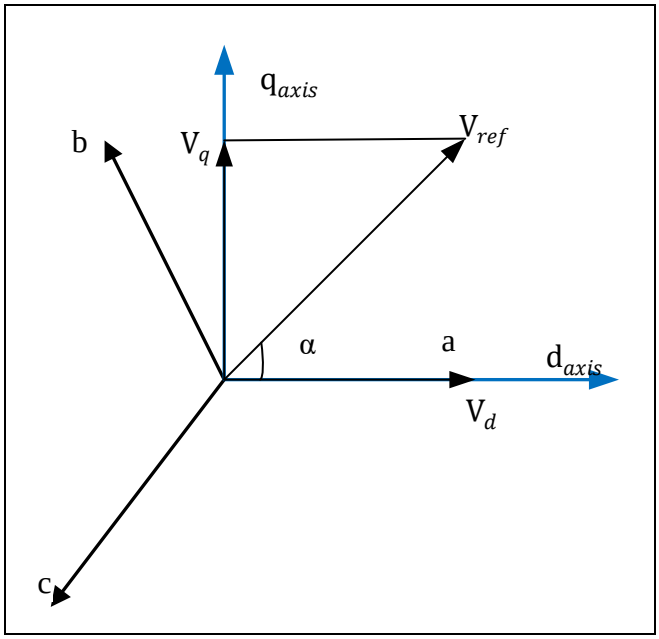

Figure 3.7 Voltage Space Vector and Its Components in (d, q).

The switching period at any Sector can be calculated as follows

$$T_1 = \frac{\sqrt{3}T_z . V_{ref}}{V_{DC}} \sin(\frac{\pi}{3} - \alpha + \frac{n-1}{3}\pi) \quad 3.37$$

$$= \frac{\sqrt{3}T_z V_{ref}}{V_{DC}} \sin(\frac{n}{3}\pi - \alpha) \quad 3.38$$

$$= \frac{\sqrt{3}T_z . V_{ref}}{V_{DC}} (\sin\frac{n}{3}\pi \cos\alpha - \cos\frac{n}{3}\pi \sin\alpha) \quad 3.39$$

$$T_2 = \frac{\sqrt{3}T_z . V_{ref}}{V_{DC}} \sin(\alpha + \frac{n-1}{3}\pi) \quad 3.40$$

$$= \frac{\sqrt{3}T_z . V_{ref}}{V_{DC}} (-\cos.\sin\frac{n-1}{3}\pi + \sin\alpha \cos\frac{n-1}{3}\pi) \quad 3.41$$

$$T_0 = T_z + T_1 + T_2, \text{where n is the sector and } \alpha \text{ is } 0 \leq \alpha \leq 600 \quad 3.42$$

3.3 Simulation Result

MATLAB/ Simulink model of 250 Hp, 2575 V, 4-pole SPM machine is considered to illustrate the proposed modified DTC-SVM control scheme. The parameters of the SPM are shown in Table 2.2.

3.3.1 Starting Mode

Through starting mode, the actual electromagnetic torque (T*) is compared with the estimated electromagnetic torque. The actual torque tracks estimated torque as shown in Fig. 3.8 (i) generates a rated torque of 494.49 Nm at 3600 rpm (Fig. 3.8 (ii)). The stator current waveform under the starting condition is shown in Fig. 3.8 (iii) with less distortion. Also, the Dc bus voltage and the controller output frequency resulted as expected. Both output frequency and DC bus voltage produced more ripples in the DTC application and the ripple smooths the up in modified-DCT application as shown in Fig. 3.9 (i) and (ii) respectively. The desired frequency tracks the estimated frequency and reaches the maximum value.

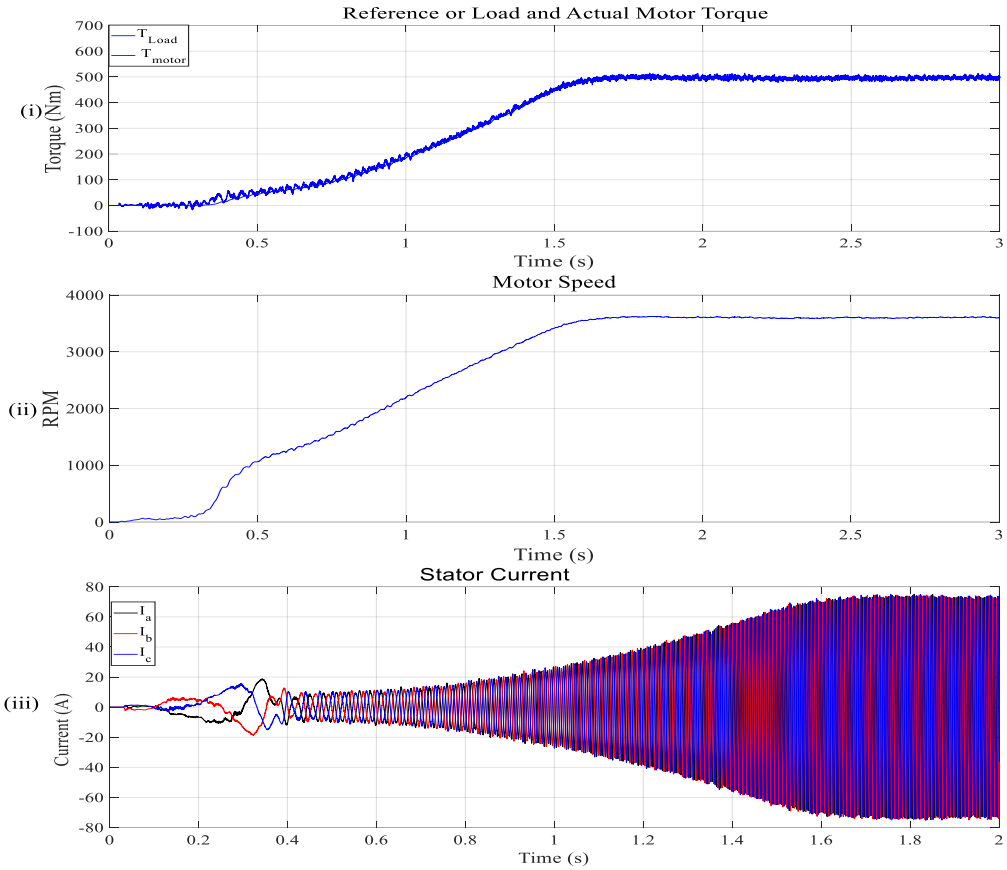

Figure 3.8 Motor Torque, Motor Speed, and Stator Current SVM in the Starting Process

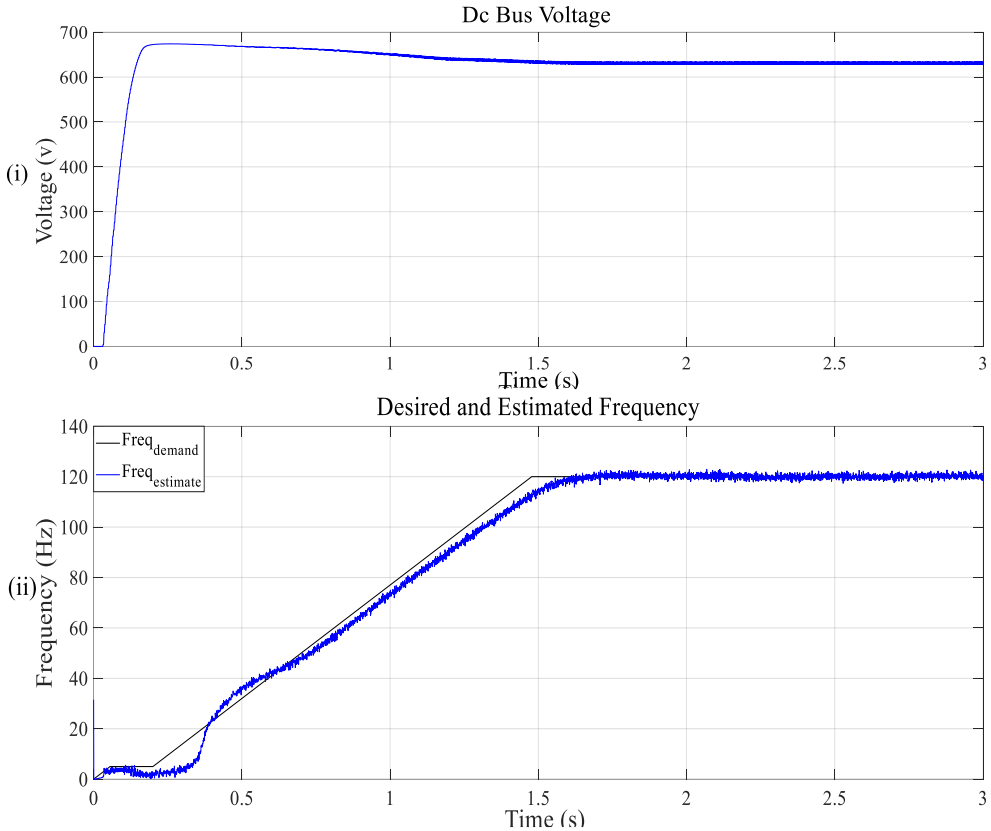

Figure 3.9 DC Bus Voltage and Controller Output Frequency SVM

3.3.2 Steady State Mode

The steady-state performance torque, speed, stator current, dc bus, and controller output frequency when the PM machine runs at 3600 rpm with a full load is shown in Fig. 3.10. The torque ripple for Modified DTC-VSM is approximately 10 Nm which is 50% lower than that of the DTC as shown in Fig. 4.10 (i). The stator current waveform under this condition generates low current distortion with a Total Harmonic Distortion (THD) of approximately 4%. The AC ripple in the DC bus reduces below 5% and the controller output frequency runs very stably in full load steady state as shown in Fig. 4.11 (i) and (ii)).

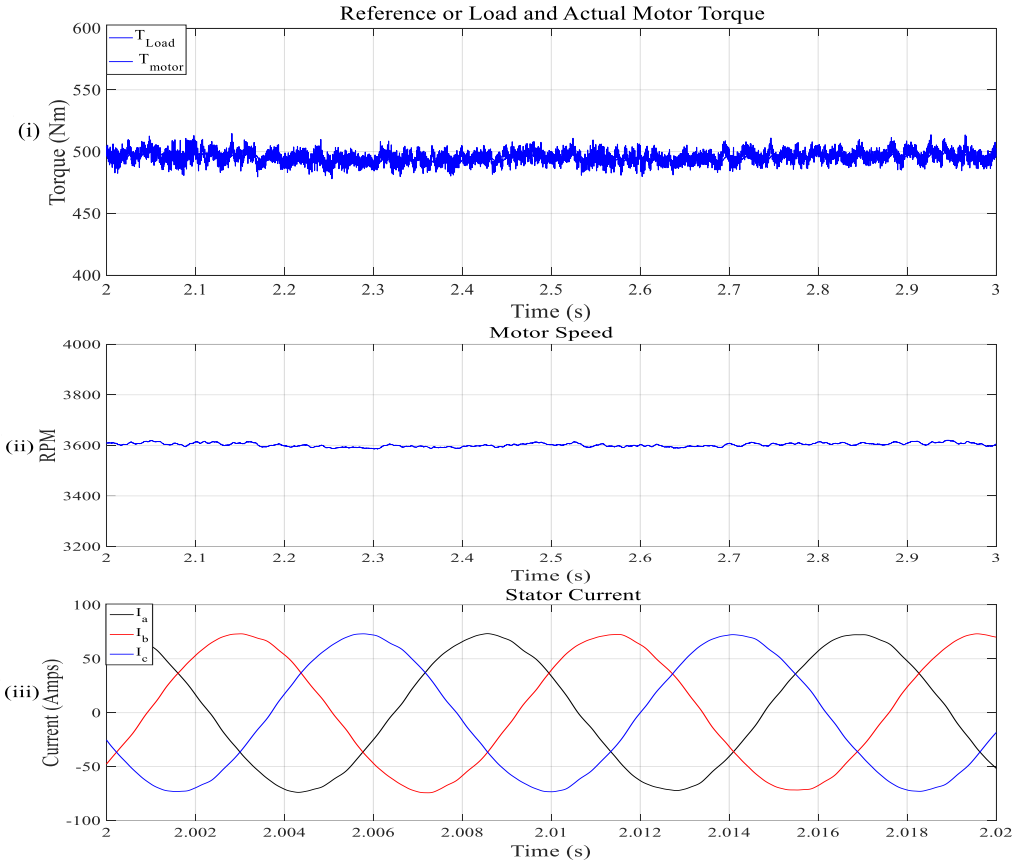

Figure 3.10 DTC-SVM steady state Torque, Speed, and Stator Current at 3600 rpm

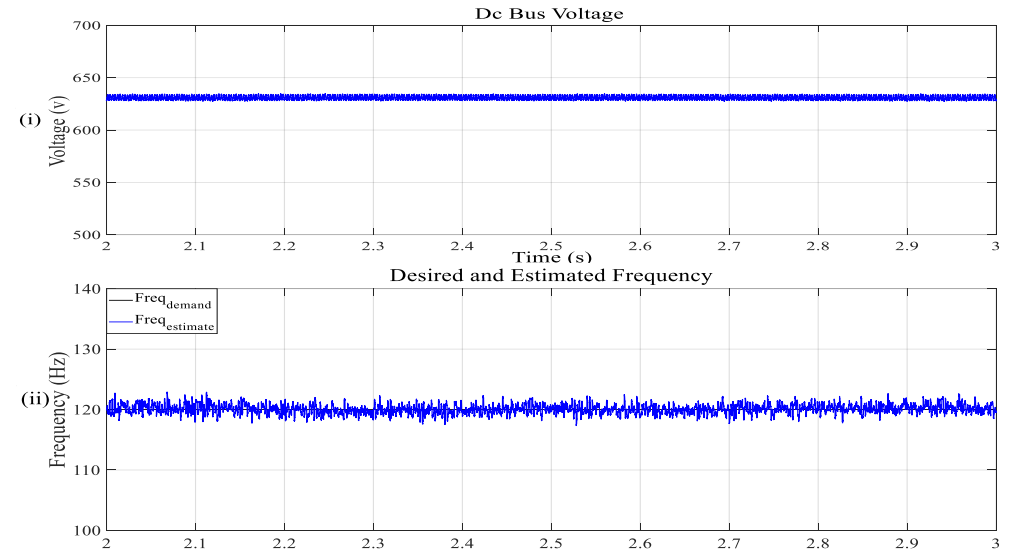

Figure 3.11 DTC-SVM steady state DC Bus Voltage and Output Frequency at 3600 rpm.

3.4 Conclusion

In this chapter, the proposed modified DTC-SVM controller for the SPM machine is presented. This control scheme has been analyzed and verified with simulation. Initially, the relationship between the stator flux linkage, electromagnetic torque, controller voltage, and current is analyzed and designed. After developing self-governing closed-loop torque and stator flux linkage control was attained by using two PI controllers. Next, the reference voltage vectors are generated using the SVM. Finally, the simulation result validated the robustness and fast torque response of the modified DTC-SVM design. The simulation results showed that the DTC with the SVM concept had been successfully extended to the ESP application. The proposed design achieves lower ripples of current and torque are both achieved while maintaining constant switching frequency with the proposed scheme. Compared to the classical direct torque control scheme proposed in the previous chapter, this scheme is a little bit more complex and slower due to the PI controls. However, the PI controller shows robustness in both starting and steady state conditions.

Chapter 4: ESP System Modeling and Analysis of Modified DTC-SVM

4.1 Introduction

The analysis and modeling of an ESP system require an intensive examination of each component within the system. Over the past ten years, the Electrical Submersible Pump (ESP) industry has seen a marked main increase in the application of PM machines with VSDs [74]. Over that same period, the complexity and diversity of the control system of VSD increased as well. To properly control the PM machine in this demanding environment, users need a greater understanding of the available VSDs options. Two configurations are typically used in ESP applications a Low-Voltage (LV) VSD with a step-up transformer to obtain the preferred voltage at the motor terminal and a Medium-Voltage (MV) VSD without a step-up transformer [75]. This section focuses on the low voltage VSD applications. ESP systems also include a multiple-stage

centrifugal electric submersible pump, an electrical submersible motor, and a downhole cable, connecting to the surface variable speed drive and transformers as shown in Fig. 4.1

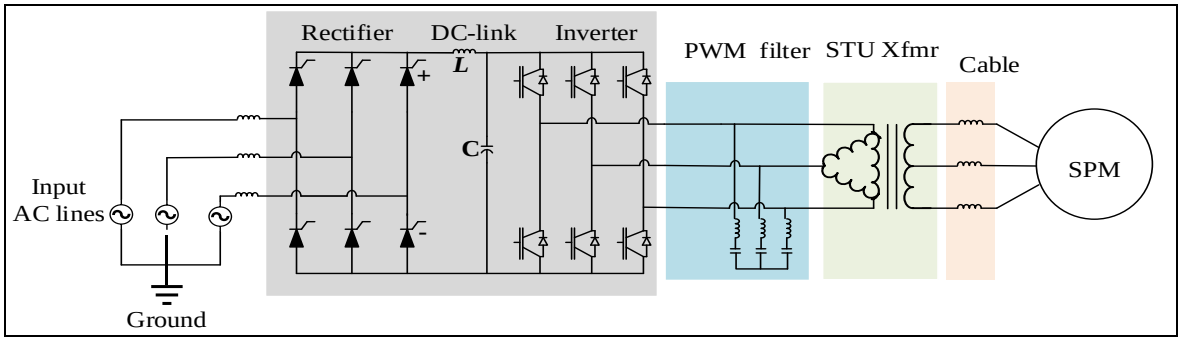

Figure 4.1 ESP System Assembly

Differential equations that describe the physical dynamics of each driven element are utilized to produce a complete system model. By resolving the equations of each major element of the system into a set of differential equations for digital integration, the system is set up to converge value at each point in time. This process numerically solves system dynamics, accounting for the differential equations that describe the coupling between the different sub-systems, [77] which greatly simplify the overall task of simulation while maintaining simulation precision.

4.1.1 Pump Modeling

A load of a centrifugal pump is dependent on the angular velocity of the pump. The development of the relationship between load vs. angular velocity will not be presented in this dissertation, simply utilized. The torque required to turn the pump increases as the square of the angular velocity, hence, the power increases as the cube. To utilize this relationship, a reference

point must be established. The power required by the pump at the rated RPM is produced by a motor at 60 Hz. From this, the torque is calculated at that RPM and then modified according to the square of the ratio between the actual RPM and the RPM for which the torque is known. The torque equation is given below

$$T_{60} = \frac{\mathrm{HP}_{60} * 746}{\omega_{60}} \tag{4.1}$$

where, the torque is in Nm, and the speed is in radians/sec. Torque as a function of angular velocity is expressed as:

$$T(\omega) = T_{60} * \left(\frac{\omega}{\omega_{60}}\right)^2 \tag{4.2}$$

Therefore, the power delivered by the pump into the fluid (in Horsepower) is

$$\mathrm{HP}(\omega) = \frac{\mathrm{T}(\omega) * \omega}{746} = \frac{\mathrm{T}_{60}}{746 * \omega_{60}{}^2} * \omega^3 \tag{4.3}$$

These equations must be evaluated utilizing the average angular velocity across all pump stages at each step-in time. The Torque load then feeds the torsion system which couples the mechanical pump system to the electromagnetic system via the shafts and impressed torque from the magnetics.

4.1.2 Motor Modeling

The motor is modeled in section 3.2. The motor consists of windings that are placed perpendicular to one another on the x and y axes. These are referred to herein as the direct axis (x), and the quadrature axis (y), and are conveniently represented by complex numbers, that is, numbers with real d-direct axis and imaginary q-quadrature axis values. Currents are considered to have d and q components as they produce a magnetic field and force on the d and q axes. The current direction is into or out of the dq plane.

As presented in session 3.2 of this dissertation, the set of equations that describe the electromagnetic operation of a motor is:

$$v_{ds} = R_s \acute{\imath}_{ds} + L_s \frac{d\acute{\imath}_{ds}}{dt} - L_s \omega_r \acute{\imath}_{qs} \quad 4.4$$

$$\psi_{ds} = L_s \acute{\imath}_{ds} + \psi_m \quad 4.5$$

$$v_{qs} = R_s \acute{\imath}_{qs} + L_s \frac{d\acute{\imath}_{qs}}{dt} - L_s \omega_r \acute{\imath}_{ds} + \omega_r \psi_m \quad 4.6$$

$$\psi_{qs} = L_s \acute{\imath}_{qs} \quad 4.7$$

$$v_{\alpha s} = R_\alpha \acute{\imath}_{\alpha s} + L_s \frac{d\acute{\imath}_{\alpha s}}{dt} - \omega \psi_m Sin(\theta) \quad 4.8$$

$$\psi_{\alpha s} = L_s \acute{\imath}_{\alpha s} + \psi_m Cos(\theta) \quad 4.9$$

$$v_{\beta s} = R_s \acute{\imath}_{\beta s} + L_s \frac{d\acute{\imath}_{\beta s}}{dt} - \omega \psi_m Cos(\theta) \quad 4.10$$

$$\psi_{\beta s} = L_s \acute{\imath}_{\beta s} + \psi_m Sin(\theta) \quad 4.11$$

4.1.3 Cable Modeling

The ESP cable is usually several thousand feet and thus there will be a significant voltage drop due to the resistive and inductive impedance of the cable. The cable conductors do not have a constant inductance but rather depend on the instantaneous currents of each one of the three phases [76]. Each conductor goes through an inductance cycle as the power goes through a complete cycle. For the cable, the average inductance of each conductor can be used. In most cases, the flat cable is used rather than the round cable. Flat cable has a very different inductance cycle for the center conductor than the outer conductors [78]. This unbalances the currents in the motor and it is included in the simulation.

The first thought for incorporating the cable resistance and inductance into the system is to simply add it to the stator inductance and resistance. This will yield improper results because

these values are not physically a part of the motor. The system inherently makes them a part of the motor dynamics and while the results are close in the steady state, they are incorrect during transients. The actual circumstance is a motor driven through a series R L impedance. The voltage drop across this impedance is dependent on the current. The relationship is in the Laplace domain.

$$V_{drop} = (R + L * S)I \tag{4.12}$$

where S is the Laplace operator

The motor system is accomplished by the iterative process given below:

$$V_{motor} = V_{surface} - (R + L * S) * I_{motor} \tag{4.13}$$

$$Vm_j = Vs_j - (R + \frac{dL}{dt})I_j + \frac{L}{dt} * I_{j-1} \tag{4.14}$$

4.1.4 Step-Up Transformer

Another common requirement in ESP applications is the use of a step-up transformer. These are used to provide isolation between the down-hole ESP system and the surface equipment and to provide adequate voltage to the motor. The transformer ratio or taps in the case of the multiple-tap transformer selection is based on the ratings of both the drive and the motor, maximizing the available kVA use of the drive. The use of a transformer also allows for the same drive to be used in multiple applications and with multiple motors by using multiple-tap transformers, this is of great value as not all ESP motors have the same voltage ratings, and not all pump depths are the same.

4.1.5 PWM Sine Wave Filter

PWM modulation is a common method for providing voltage to a machine and it allows for accurate and fast control of the frequency and amplitude of the desired fundamental

component. The capacitance of the cable produces a negligible effect unless a direct PWM waveform is applied at the surface. However, in ESP applications, PWM sine-wave filters are necessary due to the long ESP cable and high dv/dt created by the inverter in the VSD [79]. The high dv/dt occurs when the IGBTs turn ON and OFF to create the required PWM modulation. PWM should never be used with long cables since the voltage reflections build and can cause extremely high voltages at the motor which breaks down the insulation [80]. PWM waveforms will be properly filtered, and the system considers only the resistance and the inductance of the cable. While in the absence of a filter, the current is nearly sinusoidal due to the inductance in the cable, voltages could result in higher than nominal peak values which can damage motor and cable insulation and can result in premature failure of ESP components.

In common dv/dt filters design, voltage clamping is specified to be at 150% of DC bus voltage at 100 feet. 480-volt systems designed will reduce the voltage at a magnitude below 1000 volts peak. This will help to reduce voltage reflection which contributes to reduced motor stress.

In most industrial drive applications, the surface motor is located relatively close to the drive, and the electrical characteristic of the drive is dominated by the motor load. With the submersible motor and pump, this is not the case. Cable lengths can be varying from virtually 0 to over 20,000 feet. There almost always is a step-up transformer between the motor and the drive to obtain the preferred terminal voltage. The impedance and capacitance of the step-up transformer and long lengths of cable can play significant roles in the drive and the filter electrical load characteristics.

4.2 Control Strategies

From section 3.4 modified DTC-SVM controller stratagem is implemented based on an Altera Cyclone V FPGA with a built-in Nios II processor. FPGA-based implementation, hardware peripherals to the processor such as PWM blocks, PLLs, counters, IOs, and communication peripherals, among others, were designed and implemented in the FPGA-based platform, as shown in Fig. 4.2.

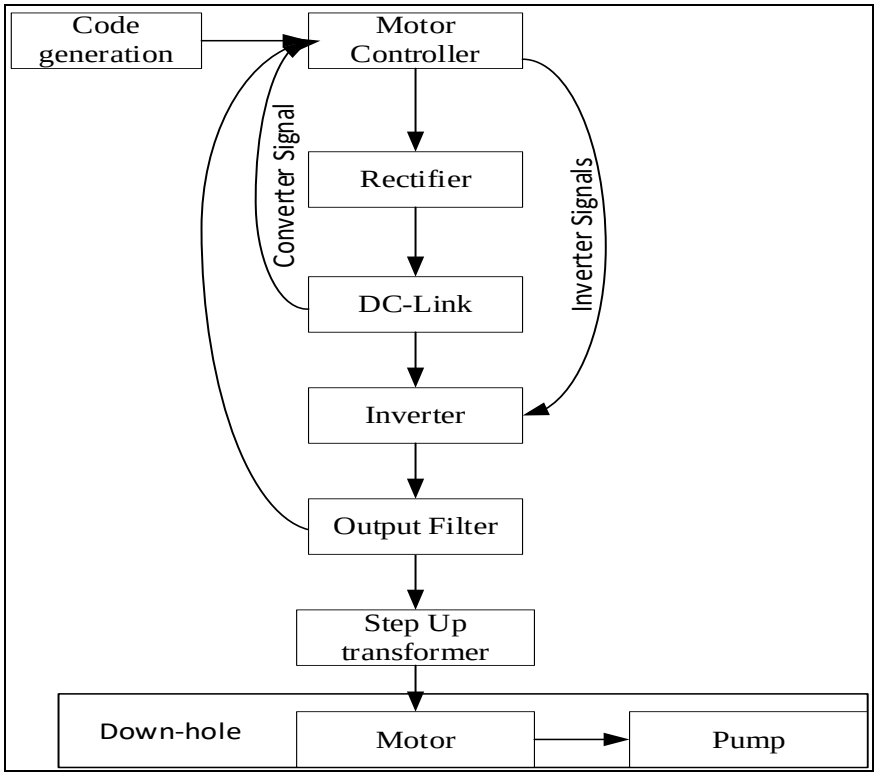

Figure 4.2 Motor Control Strategies.

4.3 Hardware-in-the-Loop (HIL) Modeling

The HIL simulation was performed in microsecond resolution with a real-time continuous interface with the switching signals generated by the analog circuits or fast digital signal processors control. The system setup is to validate robust torque reaction, and high-efficiency performance of the DTC-SVM scheme, by connecting it to the digital simulator that simulates the drive circuit, including converter 6-SCR, the DC-link, and the inverter, with 6-IGBT, the sin wave filter, the step-up transformer, the cables, and the SPM motor as shown in Fig. 4.3.

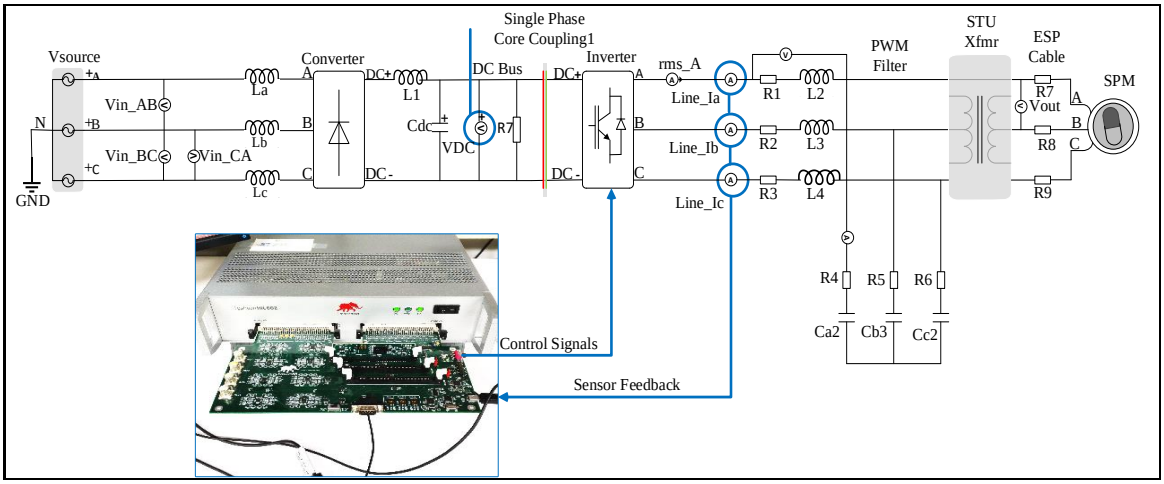

Figure 4.3 SPM System HIL Mode.

4.3.1 HIL Test Setup

The HIL system application complete setup is illustrated in Fig. 4.4. The controller includes the control module, the converter signal generator, the PWM generator, and the FPGA logic. The software is developed on the Nios II processor Altera family and implemented using Cyclone V Altera 5CEFA5F. The controller runs at 500 µs and the PWM carrier has a frequency adjusted from

2 kHz to 5 kHz. HIL application experimental setup and equipment parameters are illustrated in Table 4.1.

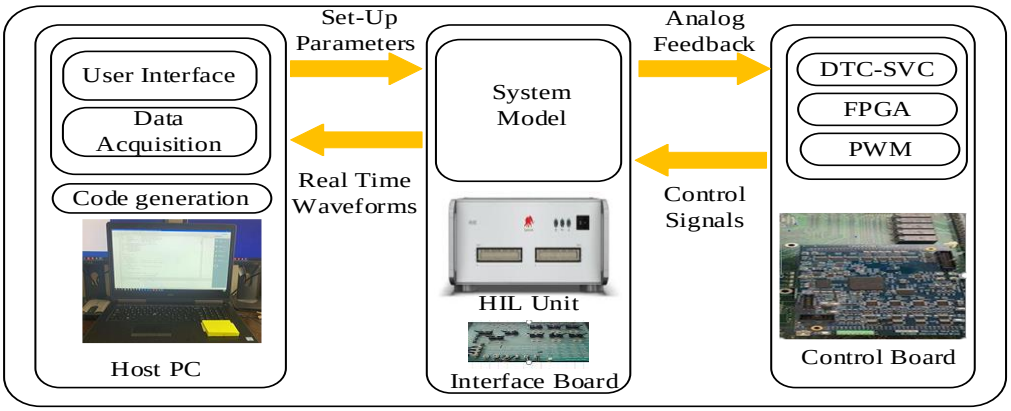

Figure 4.4 HIL Setup of the SPM Drive

Table 4.1 ESP System Parameter

VSD		SPM Machin	
KVA	520	Output Horsepower (Hp)	250
Voltage (V)	480	Voltage (Volt)	2575
Current (A)	620	Current (A)	50
Frequency (Hz)	60	Speed (RPM)	3600
Step-up Transformer		Torque (Nm)	494.5
KVA	520	Poles	4
Voltage	1200-3200	Stator resistance Rs (Ω)	1.052
Impedance (%)	3.5	Stator inductance Ld.=Lq	20
Dyno			
Horsepower (Hp)	440		

4.3.2 HIL Test Result

To validate the performance of the proposed DTC-SVM control ESP system, extensive simulations were performed using the HIL. Fig. 4.5 to 4.8 show the performance of the ESP system at 3600 rpm in different load settings. The performance of the modified DTC-SVM is exceptional because the system is stable, and motor efficiency and power factor are high in diverse load conditions

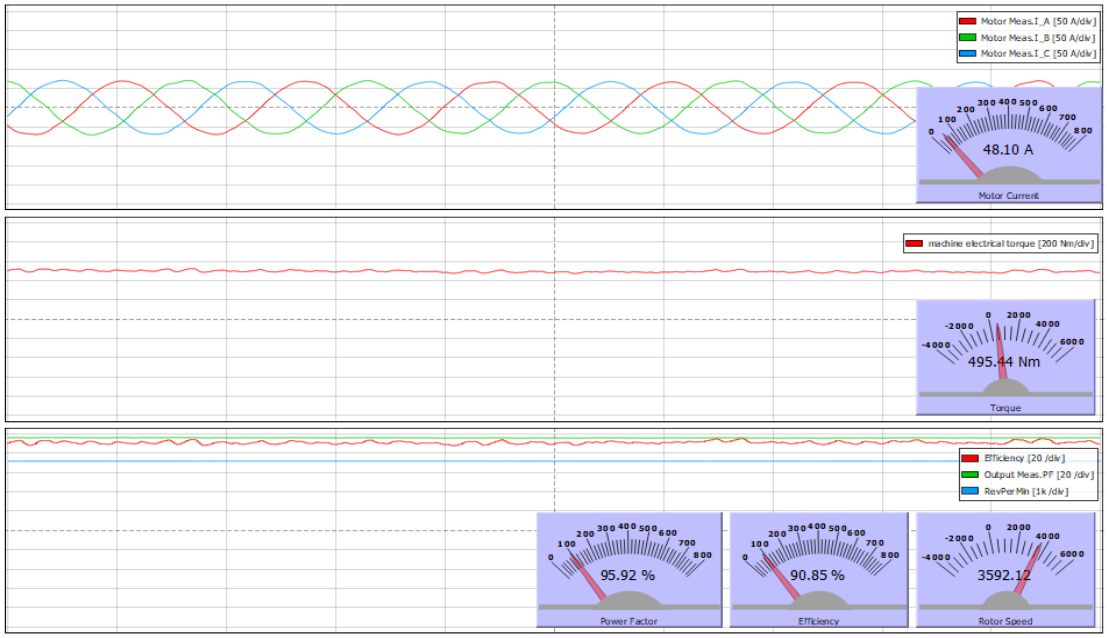

Figure 4.5 Stator Current, Torque, Speed, Power Factor, and Efficiency at 3600 rpm with 100% Load (HIL Simulation)

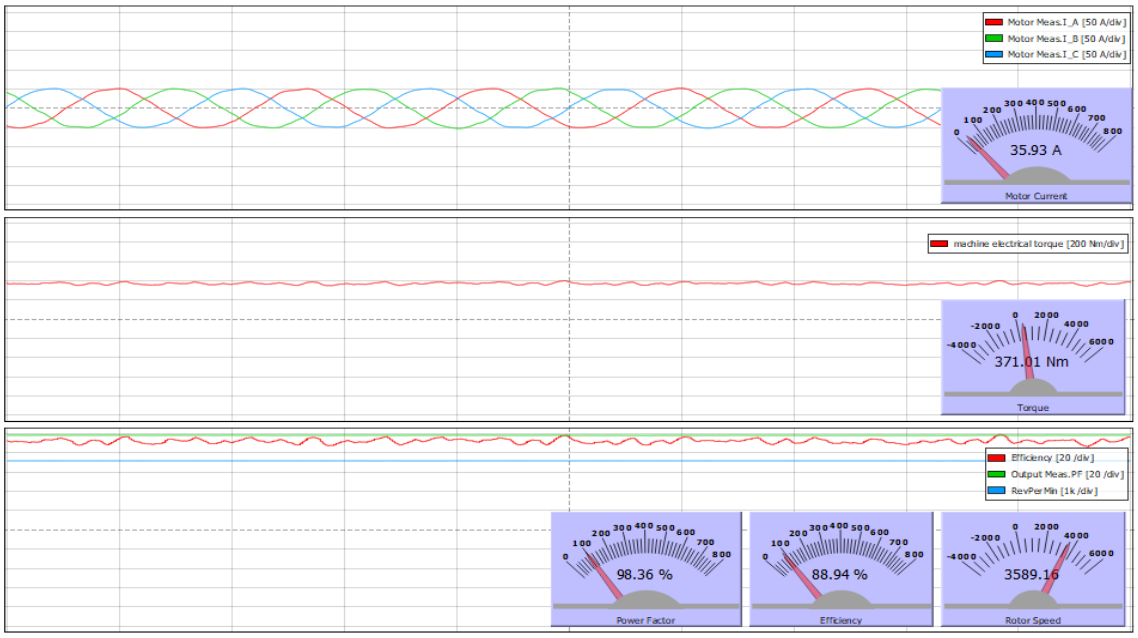

Figure 4.6 Stator Current, Torque, Speed, Power Factor, and Efficiency at 3600 rpm with 75% Load (HIL Simulation).

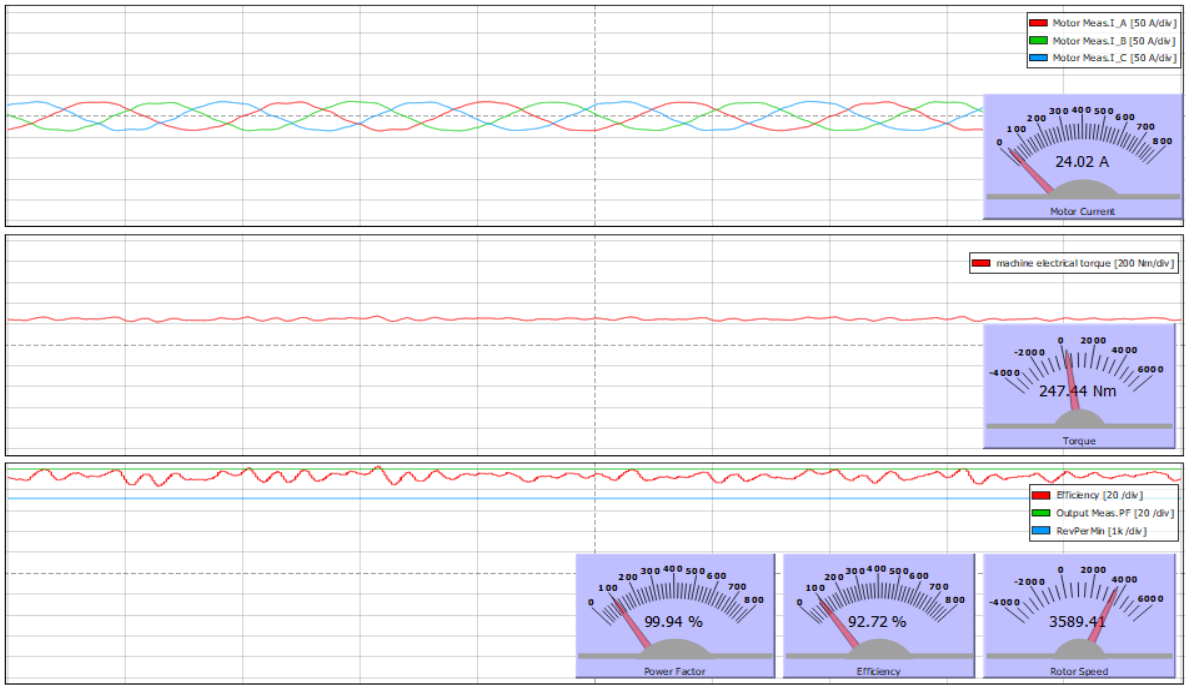

Figure 4.7 Stator Current, Torque, Speed, Power Factor, and Efficiency at 3600 rpm with 50% Load (HIL Simulation)

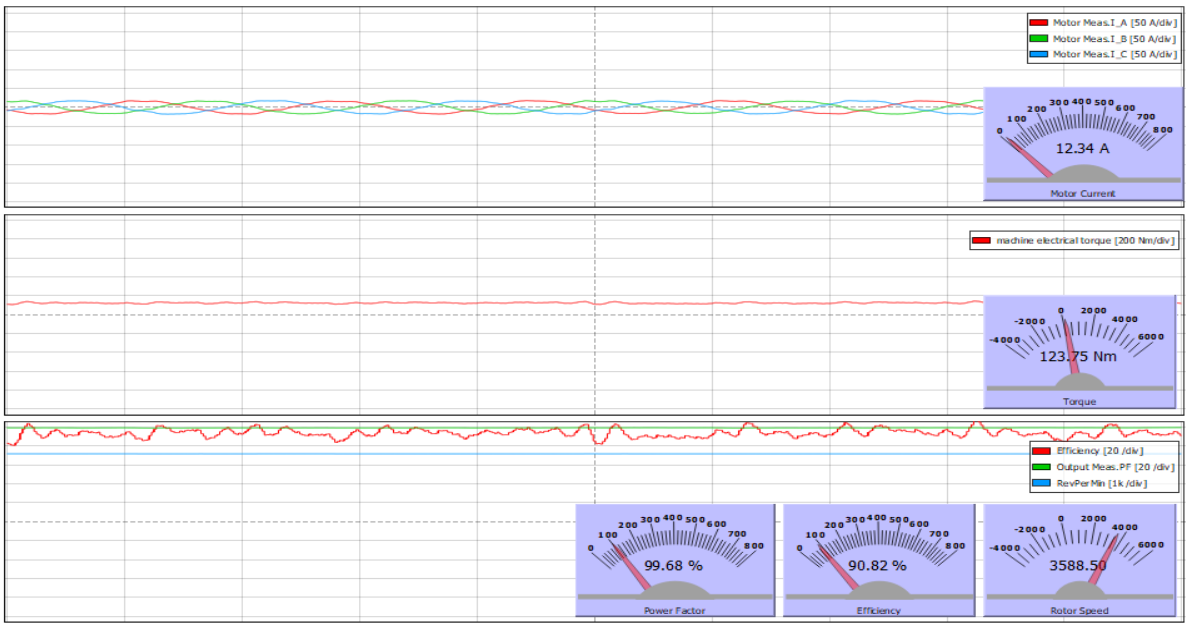

Figure 4.8 Stator Current, Torque, Speed, Power Factor, and Efficiency at 3600 rpm with 25% Load (HIL Simulation)

4.4 Experimental Setup

The proposed DTC-SVM scheme for the SPM machine is validated below. Experimental results were obtained from the practical application of the ESP drive system. Fig. 4.9 shows, the experimental setup, and the parameters used in the experiment of the SPM machine are shown in Table 4.1. Steady-state performance and dynamic performance were evaluated and compared with the simulation result.

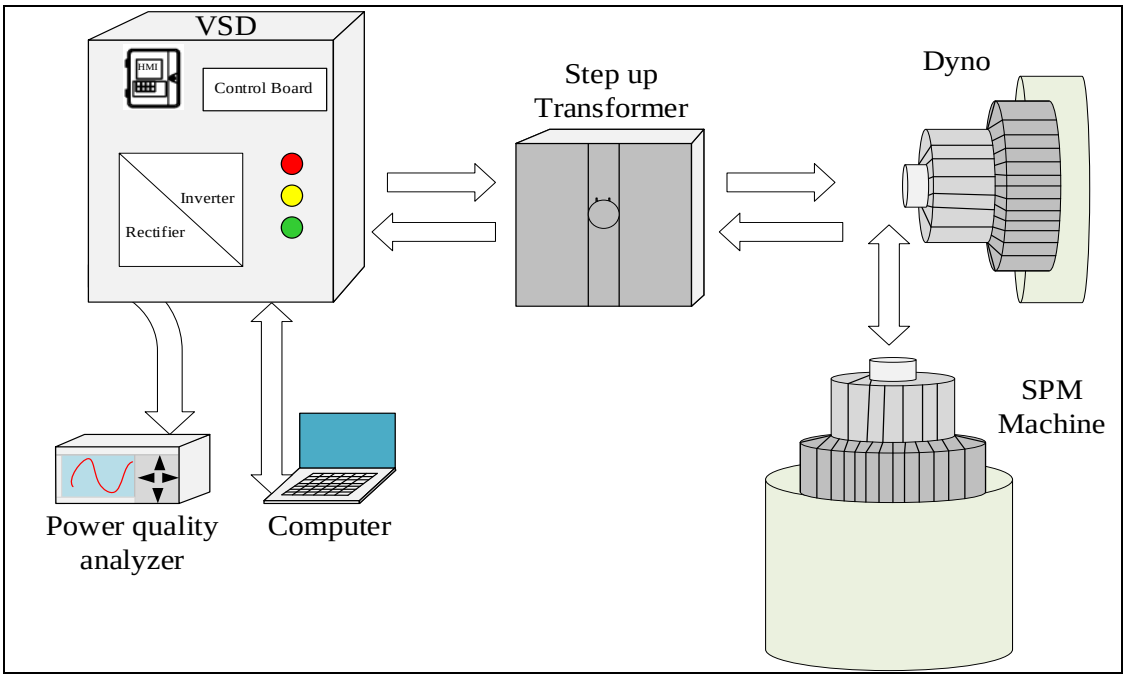

Figure 4.9 Experimental Setup

4.5 Experimental Result

4.5.1 Steady-State Performance

The steady-state performance is depicted in Fig. 4.10 to Fig. 4.12. The motor runs at 3600 rpm with 100%, 75%, 50%, and 25% load. Torque, Speed, Stator Flux linkage, and three-phase currents of the motor were monitored, and the results are shown below. The torque ripple generated was significantly small, and the current waveform shows a balanced current value and is less harmonic. The test result shows the stability of the DTC- SVM schism for different load settings.

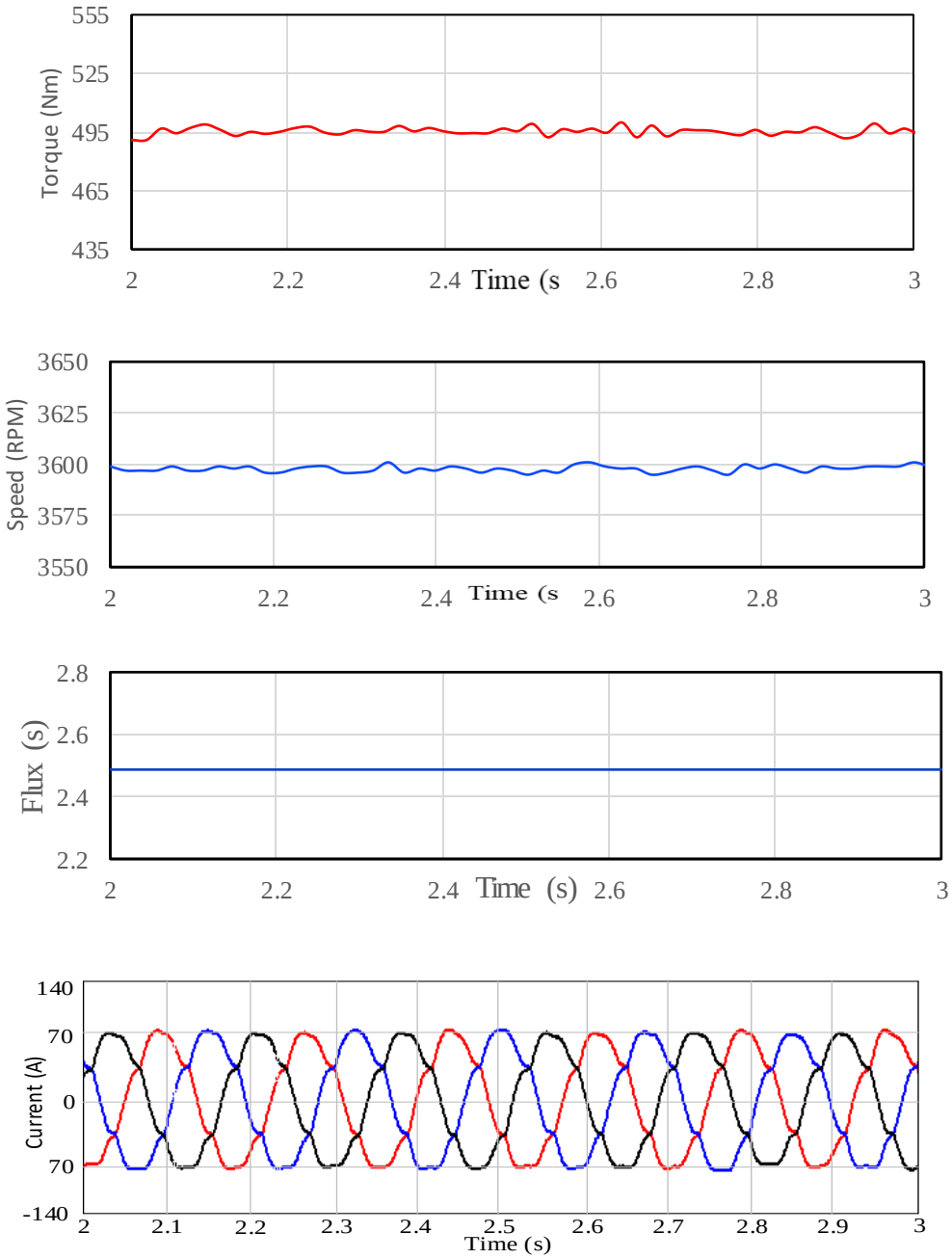

Figure 4.10 Torque, Speed, Stator Flux Linkage, and Current at 3600 rpm with 100% Load Under DTC-SVM (Experimental)

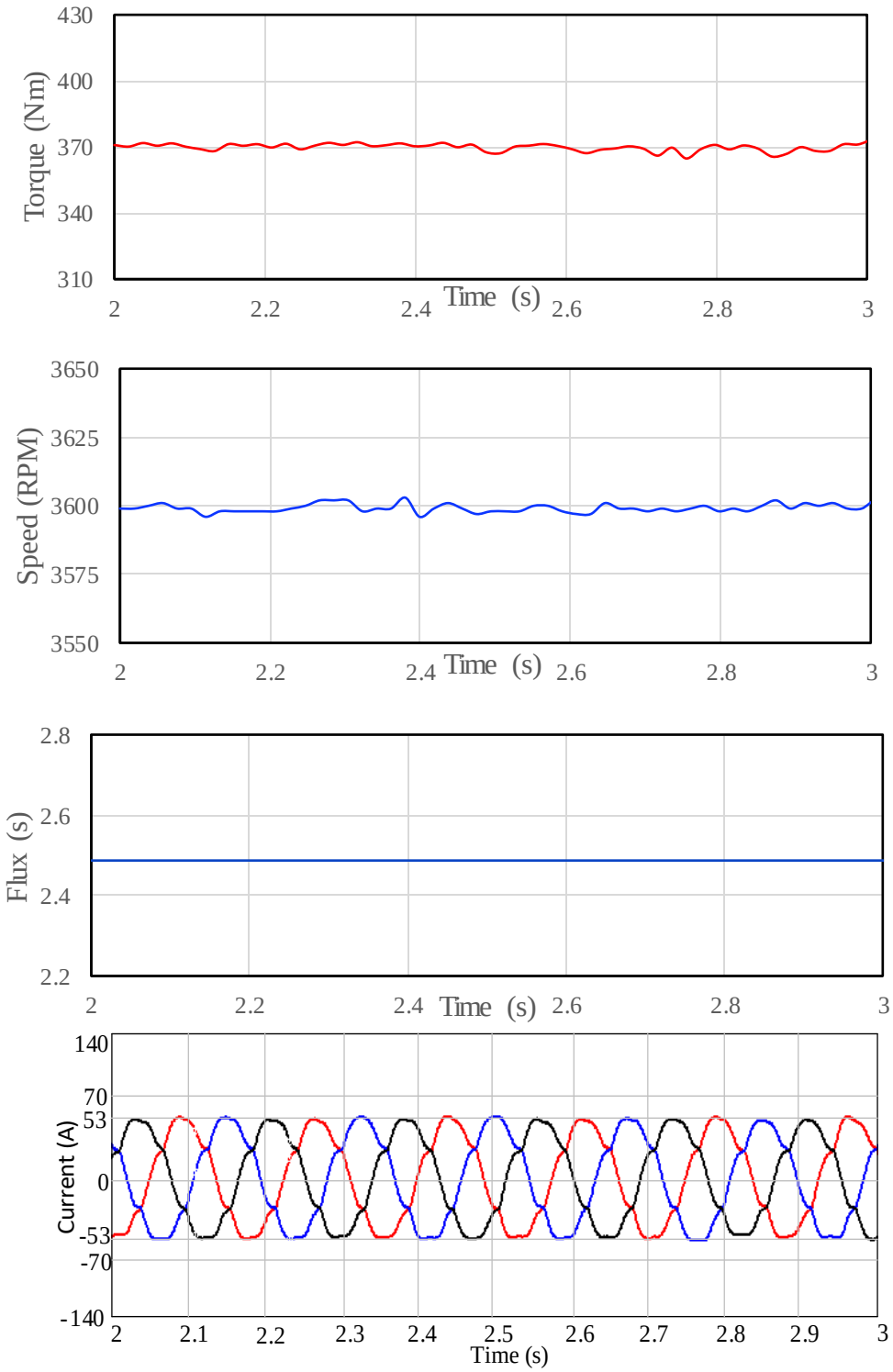

Figure 4.11 Torque, Speed, Stator Flux Linkage, and Current at 3600 rpm with 75% Load Under DTC-SVM (Experimental)

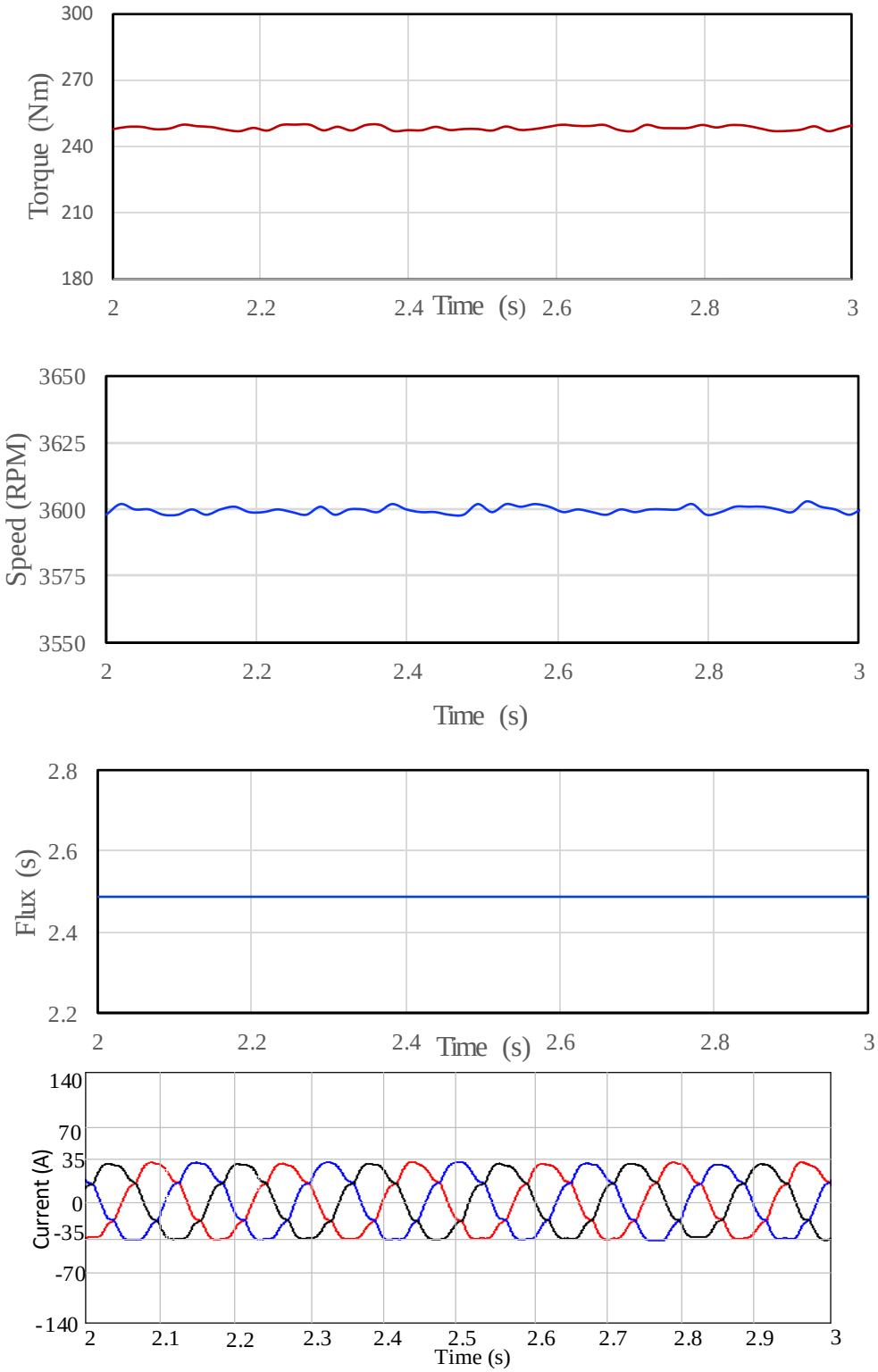

Figure 4.12 Torque, Speed, Stator Flux Linkage, and Current at 3600 rpm with 50% Load under DTC-SVM (Experimental)

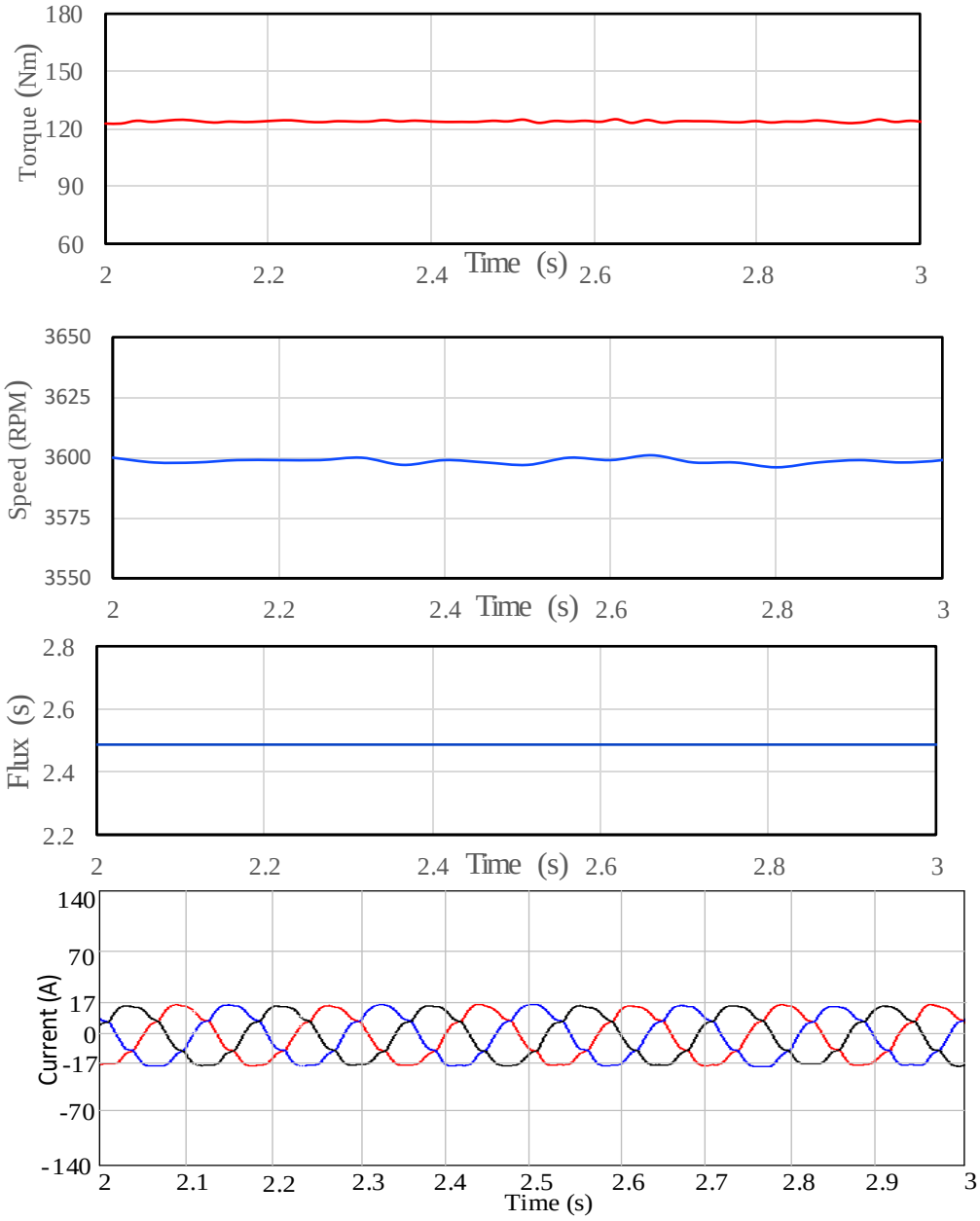

Figure 4.13 Torque, Speed, Stator Flux Linkage, and Current at 3600 rpm with 25% Load under DTC-SVM (Experimental)

4.5.2 Dynamic Performance

The dynamic performance of the experimental result is presented in Fig. 4.12 and Fig. 4.13 These results are indications of the effectiveness of the proposed control technique for SPM motion for ESP application. From Fig. 4.14 and 4.15, it can be seen that the torque and speed

track are as expected. The performance of the proposed controller showed robustness during acceleration and declaration conditions. In Fig. 4.16 the motor load increased suddenly from full load to no load back to full load. In this experiment, both speed and torque follow the reference value. It is important to do fast varying load in ESP applications since sudden load change is very common because of the good environment. In this experiment, the load was reduced from 494.5 Nm to 10 Nm in several cycles. This indicates the proposed control can handle the load variation as shown in Fig. 4.17. The measured current waveform above appeared sinusoidal, and the torque ripple Fig. 4.18 is low (~10%).

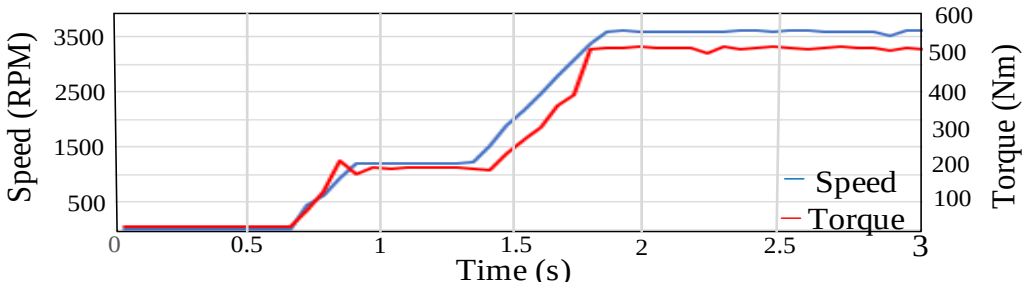

Figure 4.14 Acceleration Performances DTC-SVM (Experimental)

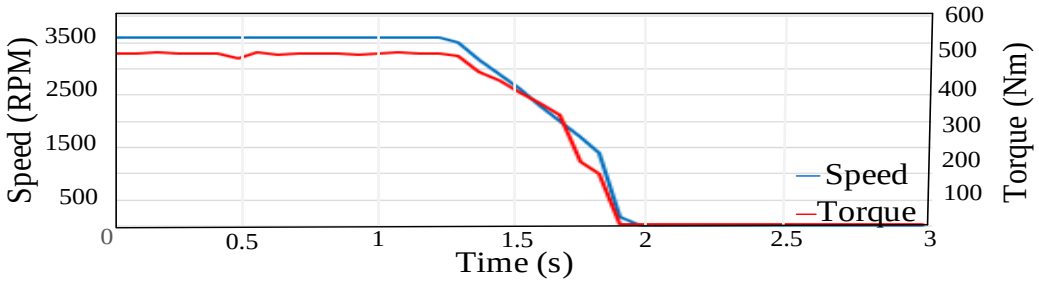

Figure 4.15 Deceleration Performances DTC-SVM (Experimental)

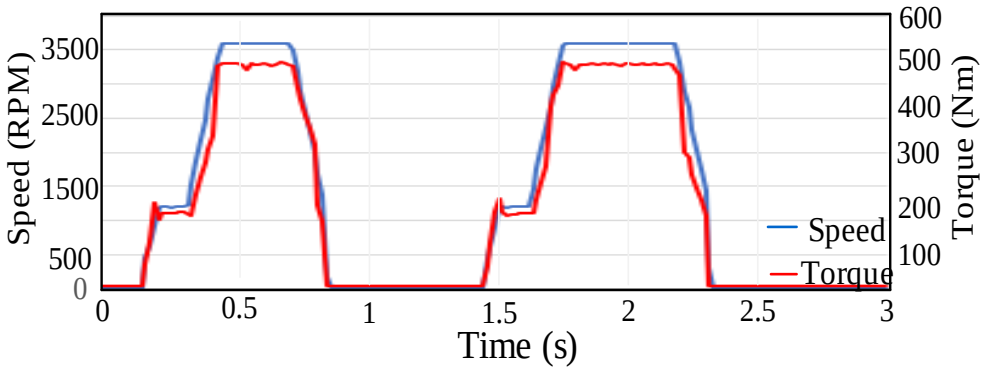

Figure 4.16 Sudden Load Change Performances DTC-SVM (Experimental).

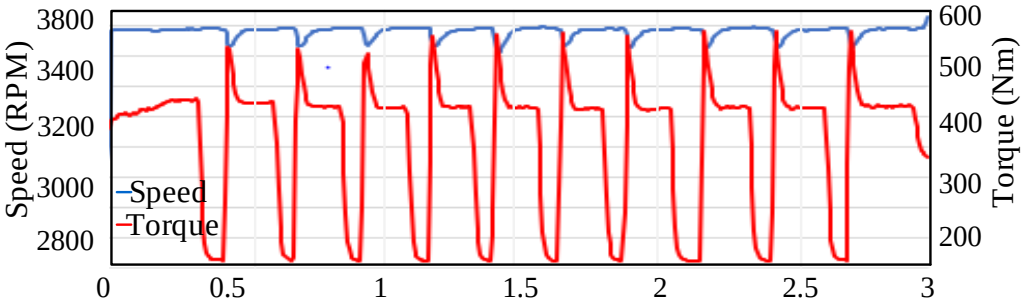

Figure 4.17 Fast Varying Load Change Performances DTC-SVM (Experimental).

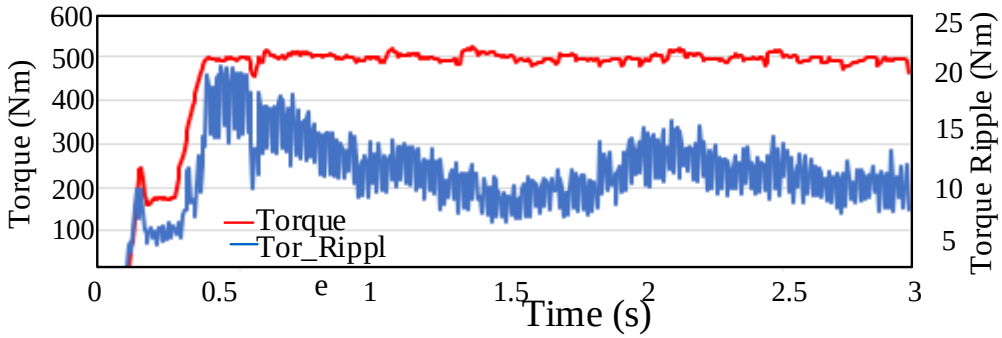

Figure 4.18 Torque Ripple DTC-SVM (Experimental).

4.6 Performance Evaluation

The performance of four control techniques evaluated in ESP system and summarized in table 4.2 below. The proposed Modified DTC-SVM scheme is compared with the classical DTC and presented in table 4.3 below.

Table 4.2 Electrical Performance for Different Control Techniques

Control Type	V/f	FOC	DTC	Modified DTC
Torque Control	No	Indirect	Direct	Direct
Flux Control	No	Indirect	Direct	Direct
Performance	Poor	High	Excellent	Excellent
Feedback required	No	Depend on	No	No
Torque response	Poor	Good	Excellent	Excellent
Accuracy	Low	Medium	High	High
Encoder	No	yes	No	No
constant switching	Yes	yes	No	yes
Torque ripples	Low	Medium	High	Low

Table 4.3 Electrical Performance DTC vs. Modified DTC-SVM

Variables	DTC	Modified DTC
Output Frequency Fluctuates (Hz)	2	Close to none
Ac Ripple DC bus (A)	7	3.5
Torque Ripple (Nm Pick)	22	10
ITHD (%)	8.5	3.8
Efficient (%)	86	92
Temp Rise (^{0}C)	4.5	2
PF (%)	85	97

4.7 Conclusion

This chapter presented the proposed modified DTC-SVM modeling and analysis of the ESP system. The proposed technique is validated in simulation and experimentally. Practical results have proved the robustness and effectiveness of this modified method for the ESP system. The control scheme has a fast speed and torque response during acceleration and deceleration time. Moreover, the effectiveness of the proposed technique remains the same in different ESP load and speed settings.

Experimental results confirm the effectiveness of the proposed control in low-speed range and the torque response has been proven robust. Fast varying of load and low torque ripple SPM control for ESP system can be achieved with modified DTC-SVM.

Chapter 5: System Efficiency Improvement

5.1 ESP System Efficiency

In an ESP system efficiency is a function of motor load, pump load as well as the mechanical requirement of the seal and gas separate. Pump horsepower is primarily a function of stage design, diameter, flow rate, fluid properties, and rotational speed. VSD can play important role in system electrical efficiency improvement by supplying appropriate voltage and frequency for the required load. Efficiency can be optimized in numerous ways such as reduced electric cost per barrel of fluid, increasing fluid production for the same electric cost, and combining the optimization of electrical cost and fluid production. In this section, we focus on reducing the electric cost per barrel (kW-hr/BFPD) which can be achieved by reducing the total horsepower for the same fluid production [81]. Selecting a more efficient pump and operating close to the best efficiency point (BEP) is possible.

5.2 Submersible Motor-SPM Efficiency

ESP PMM motors have uniquely designed to deliver dependable power to submersible pumps in extremely harsh and demanding environments. The most unusual aspects of their design are contained in their long, thin geometrical profile, high electrical and magnetic density, multiple segmented rotors, and multiple shaft bearings [82]. Putting those differences aside, the basic physics of electrical SPM motor performance is relatively consistent with PMM motors in general.

Fig. 5.1 illustrates the relationship between voltage, current, RPM, power factor, and motor efficiency. Particularly, the relationship between motor efficiency and motor current:

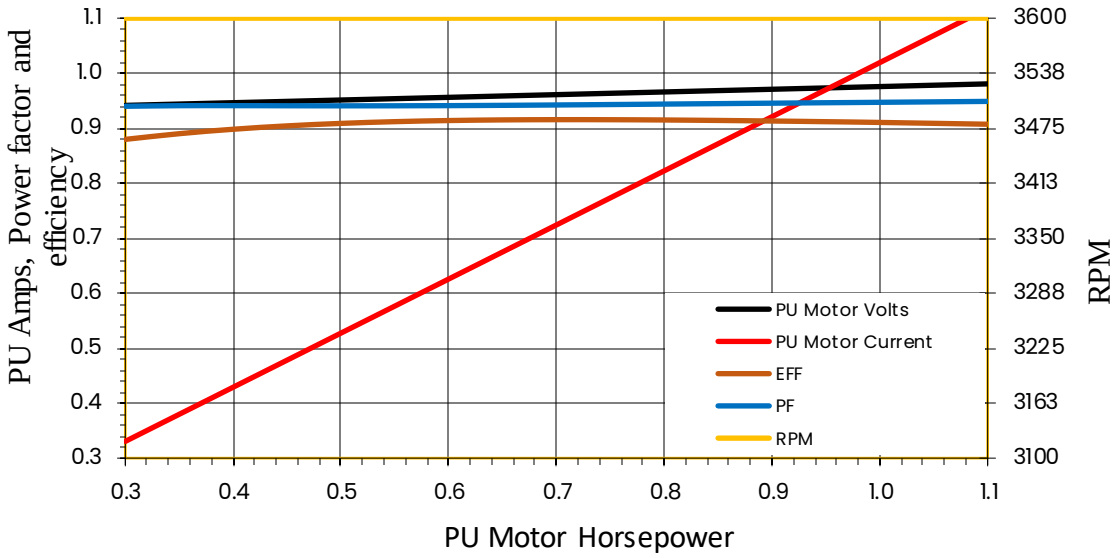

Figure 5.1 Performance Surface Permanent Magnate Motor Curves at 60 Hz.

The power consumption of a submersible motor has a direct correlation to motor operating efficiency. Whether or not the motor is operated at peak efficiency depends on the optimal voltage applied for a given load. Fig. 5.1 above, the motor is operated at the optimal voltage and delivers high efficiency and power factor over the extended operating range. Enhanced DTC-SVM SPM control operated at continual optimal voltage, this assures that the motor is operating at maximum torque and efficiency.

Advantageous to use optimized control with the highest efficiency motor, in addition to ensuring the applied voltage is optimal for the existing pump load. The high-efficiency motor consumes less energy and runs cooler because fewer losses are converted to heat.

5.3 VSD Input Power Quality Analysis

Drives must have the input Alternating Current (AC) power converted to Direct Current (DC). This is accomplished by rectification of the AC with semiconductors to produce pulsating DC which is used to charge a bank of capacitors. The capacitors then provide a constant output voltage which is utilized to synthesize output AC power of various frequencies and amplitudes as needed. Since the capacitor bank is charged to near the peak value of the rectified AC input, current only occurs in narrow pulses when the input voltage exceeds the charged capacitor voltage. The input AC voltage is sinusoidal, but the current exists as pulses. The result is a distortion of the input voltage waveform due to the pulsed current through the power source impedance. The distorted voltage on the power line then causes other equipment to operate inefficiently.

5.4 VSD Input Harmonic

In recent years, harmonic voltage and current become critical problems in electrical power systems. Hormonic is increasing continuously in industrial distribution systems due to the nonlinear loads such as VSDs. The IEEE 519 specification provides limits on the current distortion to prevent voltage distortion on the input power system. The specification sets limits on the distortion contribution of each harmonic of the power frequency and the overall current Total Harmonic Distortion (THD) [83]. THD is a measure of harmonic distortion in voltage and current waveform. The K-factor is a measure of the heating effect of the harmonic on transformers. In this dissertation, voltage, and current harmonic distortion, THD, and K-factor were measured input of VSD and the output of the PWM filter. The measured values were compared with the IEEE 519-2008 standard limits.

5.5 VSD Input Power Factor

To optimize the power factor the current and voltage harmonic waveform must be given consideration. The power factor expresses the percentage of total real power and apparent power. The inverse cosine of the power factor indicates the displacement of the current waveform concerning the voltage waveform is called the displacement power factor. Displacement is not the only reason that the real power factor can be less than apparent power. In the case of a VSD with an SCR front end, output voltage level variation is in turn controlled by the SCR converter action, and incoming voltage is available. As the firing of the SCR converter is altered about the line voltage, that determines the input current distortion and input power factor. Input power factor is maximized related to VSD load increase, as illustrated in Fig. 5.2:

$$PF = \frac{P}{\sqrt{P^2+Q^2}} = \frac{\sqrt{3}}{\sqrt{3}} \frac{V I_{out} \cos\alpha}{V I_{out}} \quad 5.1$$

when the SCR is fully phase on α = 0

$$PF = \frac{I_{out} \cos\alpha}{I_{inp}} \quad 5.2$$

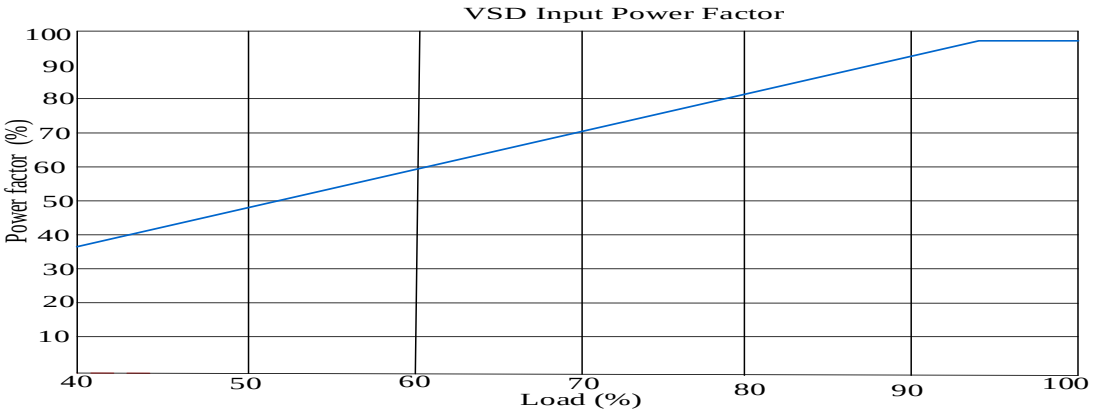

Figure 5.2 VSD Input Power Factor Related to Percentage Load

Maintaining the VSD output voltage close to the level of the incoming voltage ensures that the converter section SCRs are being operated in phase relative to line voltage. This approach improves the power factor and minimizes input harmonic distortion.

5.6 VSD Input Efficiency

The techniques for optimizing power factor tend to minimize harmonic distortion and maximize operating efficiency**.** Ensuring the VSD loading is as close to the nameplate rating as possible also ensures that the operating efficiency is maximized. The input efficiency of the VSD running 1800 rpm to 3600 rpm in the percentage of load and speed are analyzed. Fig. 5.3 illustrated efficiency values for a fully loaded VSD of 96 to 98%

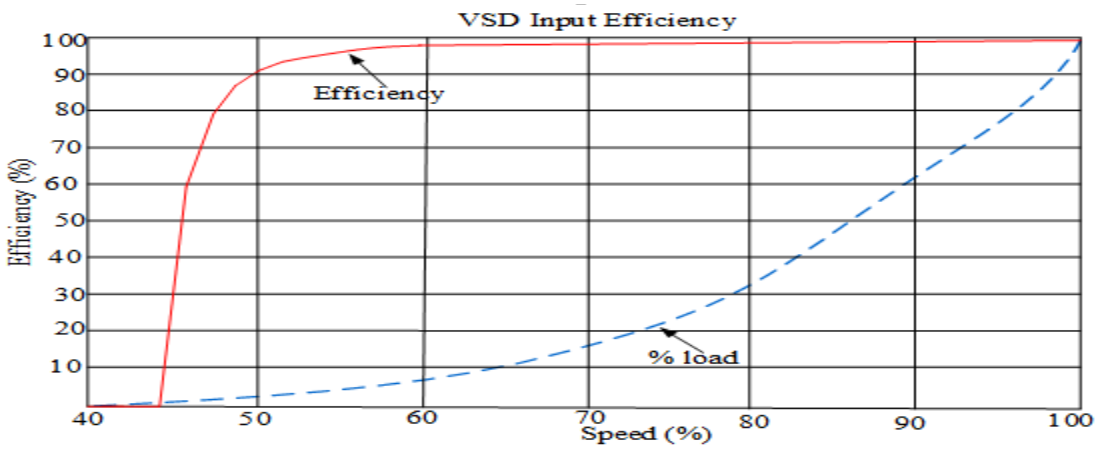

Figure 5.3 VSD Input Power Factor Related to Percentage Load.

5.7 Experimental Setup

To evaluate the efficiency and power factor of the proposed control tested with the ESP experimental platform shown in Fig. 5.4 The electrical power of VSD is obtained with Yokogawa (1800) and Fluke (435 II) power quality analyzer. The input and output power quality are measured.

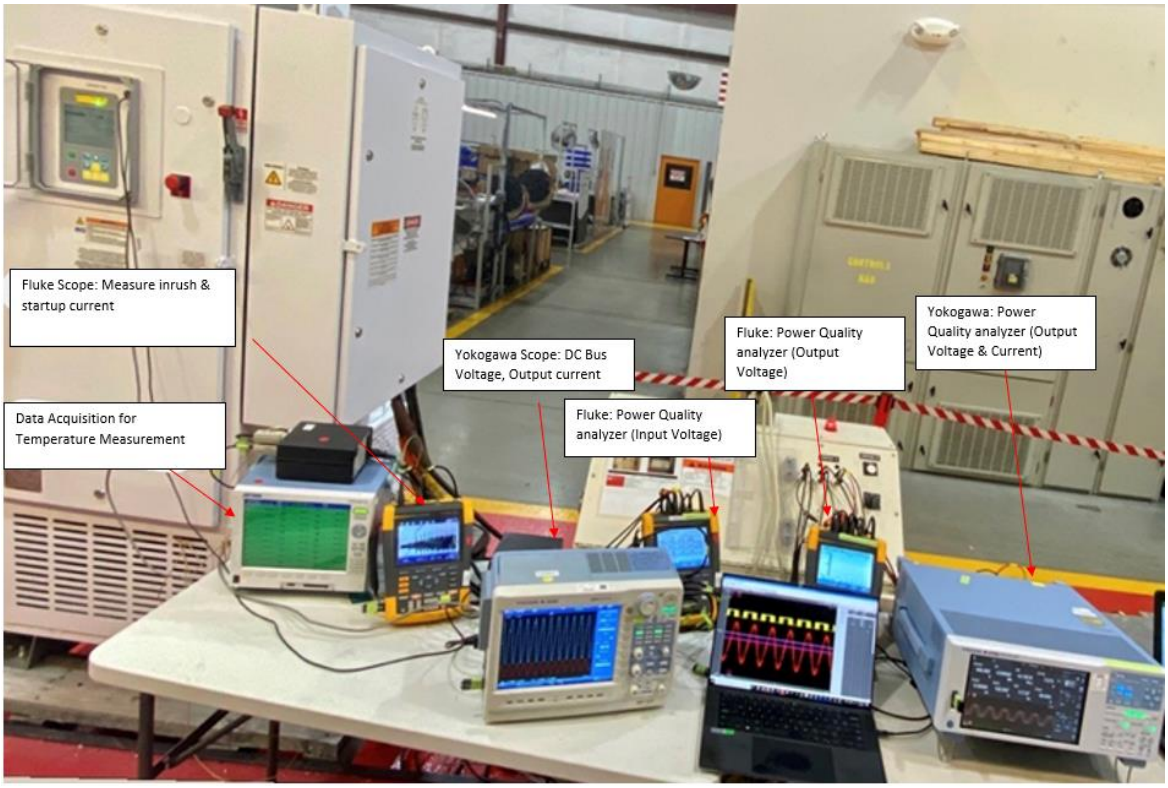

Figure 5.4 Lab Experimental Setup

5.8 Experimental Results

In this experiment 24P- 520 kVA VSD with a 24P phase shift transformer is used for harmonic cancelation. Voltage and current THD are measured at 3.8% and 3.7% respectively at full load shown in Fig. 5.5. a and b. The background voltage harmonic before the drive started was measured at 2.2% VTHD. Current and voltage THD is less than 5% within the meets IEEE 519 requests for less than 1000 kV distribution system. Power factor, kVA, and kW were illustrated in Fig. 5.6 at the drive input. Also, harmonic and temperature rises were evaluated in Fig. 5.7. Table 5.1 shows the VSD input and output power measurement.

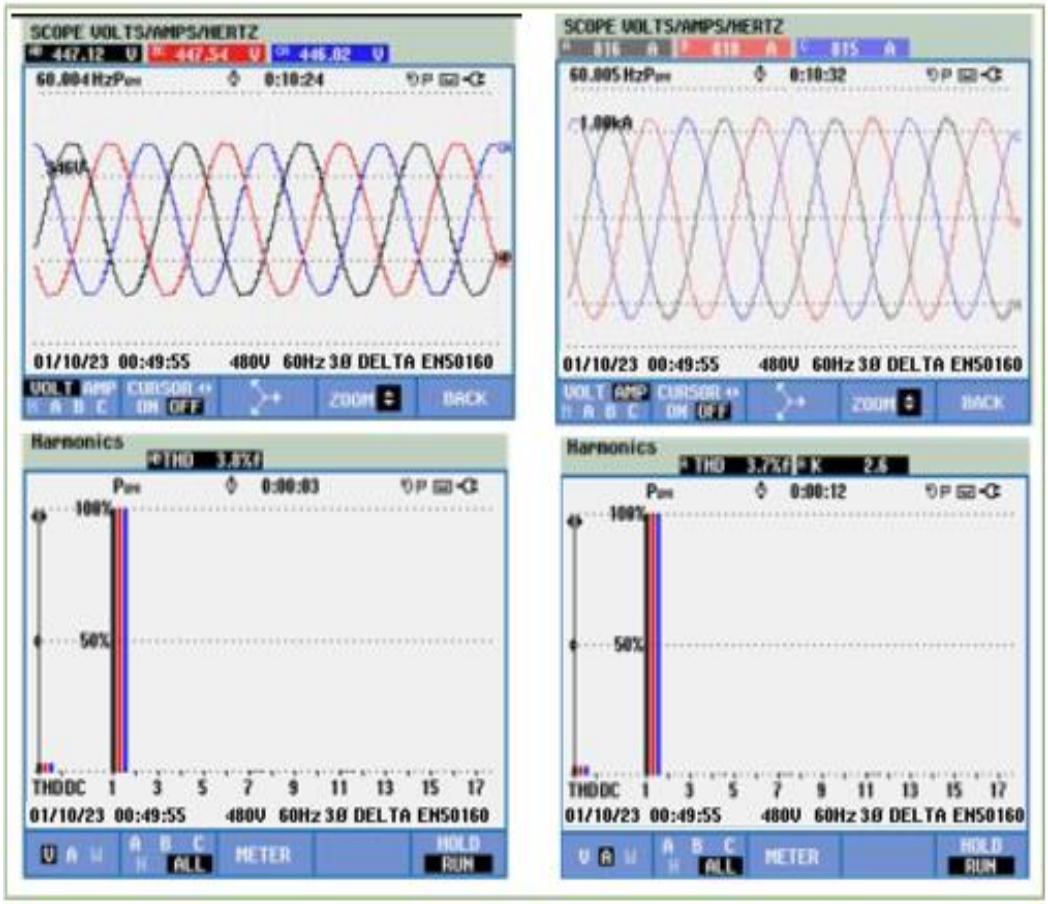

Figure 5.5 a) Voltage Waveform and THD b) Current Waveform and THD VSD Input @ 60Hz

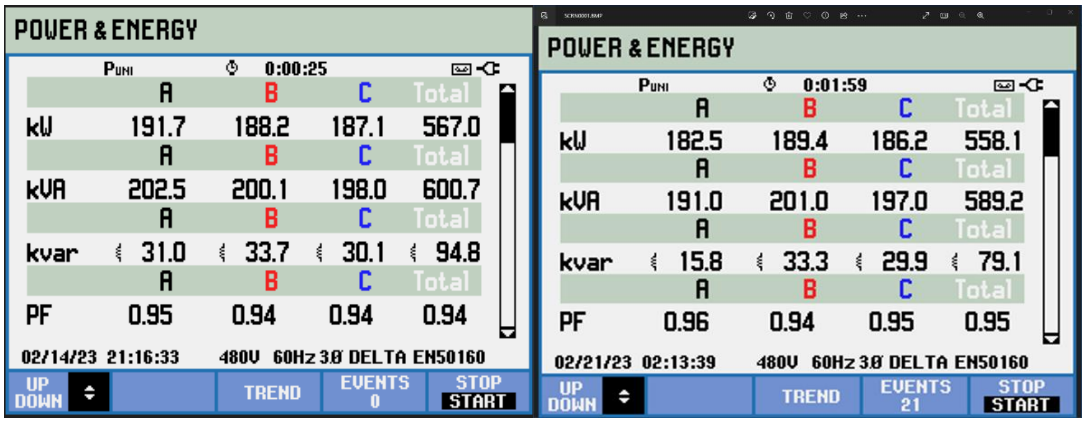

Figure 5.6 VSD Input Power Factor. (Actual Measurement was 589 kVA and 600 kVA)

Table 5.1 VSD Input and Output Power Measurement

Drive Output Frequency 120 Hz												
VSD Load	**Input**		**Output**		**THD (%)**		**K-Factor**	**kVA**	**kW**	**kVAR**	**PF**	**Eff**
	V	I	V	I	V	I						
110%	473	625	445	632	3.1	3.4		520	499.9	145.8	.96	96.9
100%	474	615	446	624	3.2	3.5	2.4	512.7	491.2	143.3	.96	97.2
75%	475	475	447	478	3.3	3.7	3.0	446.5	424.5	139.4	.95	96.5
50%	476	334	447	440	3.5	3.8	3.7	340.2	316.8	125.2	.93	95.8
25%	478	211	449	365	3.6	3.8	4.2	283.7	252.5	129.4	.89	93.8
Drive Output Frequency 100 Hz												
110%	473	535	425	523	4.8	4.6	3.5	402.2	354.0	191.1	.88	90.6
100%	474	520	416	519	4.6	4.4	3.4	400.0	344.0	204.1	.86	90.1
75%	475	415	393	391	4.2	4.3	4.2	302.2	253.7	163.9	.84	93.1
50%	478	275	379	323	4.0	4.2	4.4	251.1	203.4	147.2	.81	92.8
25%	479	187	369	287	3.8	3.9	4.5	287.6	174.4	139.9	.78	91.4
Drive Output Frequency 80 Hz												
110%	473	530	348	519	4.7	4.5	3.4	399.2	347.3	196.8	.87	89.1
100%	474	520	334	519	4.6	4.4	3.4	400.0	344.	204.1	.86	90.4
75%	476	415	319	391	4.2	4.3	4.2	302.2	254.2	164.2	.84	91.7
50%	477	275	306	250	4.0	4.2	4.4	193.4	157.1	113.7	.81	92.6
25%	478	187	298	150	3.8	3.9	4.5	132.6	103.1	82.7	.78	91.5
Drive Output Frequency 60 Hz												
110%	473	441	264	448	4.3	4.2	4.7	344.6	258.4	227.9	.79	87.2
100%	476	390	258	430	4.4	4.3	4.8	332.8	249.6	220.2	.75	88.1
75%	478	312	245	324	4.5	4.6	4.9	251.8	181.3	174.8	.72	89.7
50%	479	227	232	220	4.5	4.7	5.2	171.4	116.5	125.6	.68	92.6
25%	479	224	244	170	4.6	4.9	5.6	116.8	75.9	88.8	.65	90.7

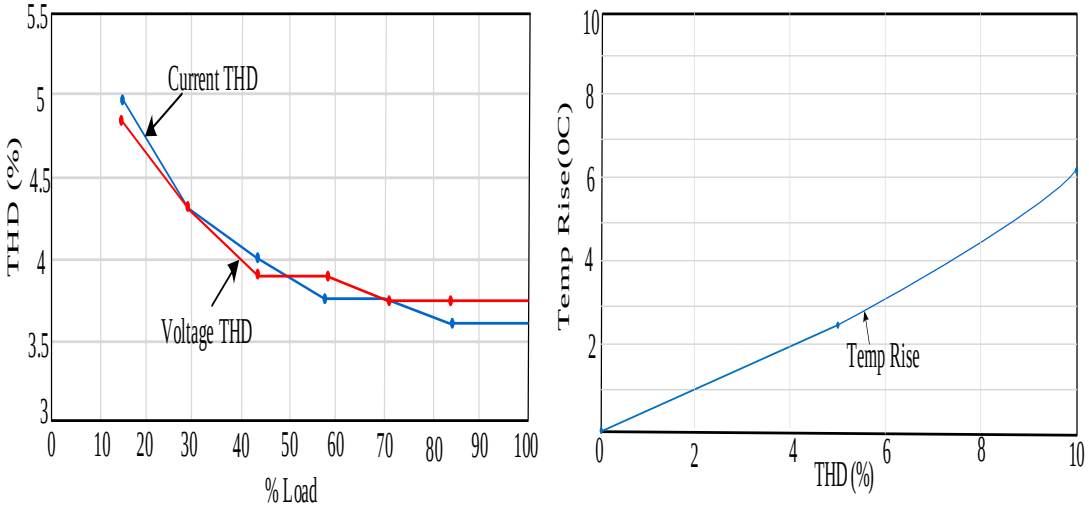

Figure 5.7 a) VSD Input Voltage and Current THD b) Temp Rise vs. Current THD

5.9 Conclusions

In this chapter, the proposed DTC-SVM control ESP system performance, and efficiency are evaluated when the VSD is running from 120 Hz to 60 Hz. The VSD is loaded from 25% to 110%. The efficiency and power factor of the VSD is shown relatively high for all load and speed ranges. The kW shows a lot of improvement with the proposed control. The efficiency and kW are directly related to the oil production power cost (kW-hr/BFPD).

Chapter 6: Conclusion and Suggestions for Future Work

6.1 Conclusion of This Dissertation

The novel DTC-SVM scheme was proposed to solve system reliability, high torque, and current ripples problem. A comprehensive evaluation of sensor-less DTC-SVC SPM motor drives has been done to achieve a number of improvements in minimizing the large torque and current ripples while maintaining a constant switching frequency. ESP system with the proposed controller was constructed and tested under different load conditions over a wide speed range, sensor-less controller obtained accurate torque and speed estimation. The controller successfully started and detected motor rotation. A summary of design, analysis, modeling, and experimental studies carried out in this dissertation and the conclusions drawn from these studies are presented in the remainder of this section.

The classical direct torque-controlled SPM machine ESP application has been analyzed and reviewed with simulation in chapter 2. The main drawback of the classical DTC is high torque and current ripples caused by look-up table of the voltage vectors and variable switching frequency by the hysteresis comparator. This problem was solved in chapter 3 whereby a novel sensor-less Direct Torque Control with Space Vector Modulation (DTC_SVM) scheme were also presented in this chapter. Two PI controllers were used to reduce torque and current ripples. Space Vector Modulation (SVN) was applied to eliminate variable switching frequency. The classical DTC fast response and robustness were fully preserved at the same time.

ESP system mode with DTC-SVM for SPM has been developed to improve the system reliability and performance in chapters four and five. The proposed technique was validated through simulation and experiment. Practical results have proven the robustness and effectiveness of this modified DTC-SVM method for the ESP system. The error between the estimated and actual values was optimized. High system efficiency, high power factors, and low torque and current ripple with low current THD were achieved with the proposed controller. Overall system stability and performance of the system were improved.

Summary, the effectiveness of the modified sensor-less Direct Torque-controlled Space Vector Modulation (DTC-SVM) for the Electric Submersible Pump (ESP)system has been confirmed and well supported by the studies presented in this dissertation.

6.2 Suggestions for Future Work

The proposed controller in this dissertation were addressed the challenges of the traditional speed range. However, in recent years the number of slim wall casing and deeper ESP installations are increased. To address challenges where traditional technologies become inadequate Ultra-High-Speed (UHS ESP) motor installation is required. Future researchers may study the effective and efficient way to control the UHS ESP motor in a wide range of operations range. Controllers require a high-speed control that can run up to 12,000 rpm. UHSESP motor also requires a high-speed sinewave filter design. It is essential to have the proper selection of carrier frequency for the sinewave filter, due to the high impact on the VSD inverter. High carrier frequency increased switching losses of the power semiconductors, which increases cooling requirements, leakage currents, and increased average power demanded from IGBT gate driver circuitry. While there are challenges and considerations to the use of higher carrier frequency,

there are also benefits such as a low THD output voltage, reduced audible noise level, reduced size, and cost of magnetic elements of PWM filter which are usually the dominant factor in the filter assembly cost.

References

[1] Evolution of ESP technology enables economical application in unconventional wells World Oil® / JUNE 2020 21

[2] Pankaj, Piyush, et al: Artificial Lift Selection and Its Applications for Deep Horizontal Wells in Unconventional Reservoirs. Proceedings of the 6th Unconventional Resources Technology Conference 2018

[3] Levi, E.: 'Multiphase electric machines for variable-speed applications', IEEE Trans. Ind. Electron., 2008, 55, (5), pp. 1893-1909.

[4] J. Feng, W. Gui, J. Xu, and J. Wang, Compare of Permanent Magnet Synchronous Motor Applied to Railway Vehicle Traction System, 2nd IEEE Conference in Industrial Electronics and Applications, pp.74-77, May 2007

[5] K. Matsuoka, Development Trend of the Permanent Magnet Synchronous Motor for Rail Vehicle Traction, Journal of the Institute of Electrical Engineers of Japan, Vo1.l26, No.2, pp.729-731, 2006

[6] Roberto, M., Oliveira, P., Pyramo, B., 2013. Mudline esp: electrical submersible pump installed in a subsea skid. In: Proceedings of the Offshore Technology Conference

[7] Gabor Takacs: Electrical submersible pumping manual, Second Edition Gulf Professional Publishing

[8] Anville Francis, Jesse Allen, Sandy Williams- "Improving ESP Run- life in a New Field (Mississippi Lime)", 2015, ESP Workshop

[9] "Recommended Practice for Electrical Submersible Pump Teardown Report: API Recommended Practice 11S1", Third Edition American Petroleum Institute, 1979.

[10] Dong Guo; Cauligi S. Raghavendra et.al: Data-driven: ISBN: 978-1-61399-404-7

[11] Analysis of vector controlled permanent magnet synchronous motor using MATLAB/ Simulink approach i-manager's Journal on Electrical Engineering, Vol. 11 l No. 1 l July - September 2017

[12] S. Noonan, "Electric Submersible Pump (ESP) Reliability," in Society of Petroleum Engineers Webinar, Houston, TX, 2013

[13] Tan Nguyen: Electrical Submersible Pump Design, Practices, and Applications Book/2020

[14] G. Takacs" Three inventions shaping the future of ESP technology" Journal of Petroleum Science and Engineering 182 (2019) 106330

[15] Gabor Takacs Electrical Submersible Pumps Manual: Design, Operations, and Maintenance (Gulf Equipment Guides) 1st Edition.

[16] Cheryl Schmehl, Mark McKinley et.al Adjustable speed drive selection for electric submersible pumps 2014 IEEE petroleum and Chemical industry Technical Conference (PCIC).

[17] Tran Huong Thuy Chu: A simulation study of ESP's failures due to motor's overheating New Mexico Institute of Mining and Technology may,2021

[18] R. L. Hyde and T. R. Brinner, "Starting characteristics of electric submergible oil well pumps," IEEE

[19] C. Concordia, "Induction motor damping and synchronizing torques," AIEE Trans., vol. 71, no. 1, pp. 364–366, Jan. 1952.

[20] Gabor Takacs: Electrical submersible pumping manual, Second edition

[21] Chad Bremner, Grant Harris et.al: Evolving Technologies: Electrical Submersible Pumps. Oilfield Review (Spring 1999): 48–63

[22] G. Takacs "Three inventions shaping the future of ESP technology" Journal of Petroleum Science and Engineering 182 (2019) 106330

[23] Dwiggins J, Hughes R, Kopecky T. Reducing production costs with permanent magnet motors. Paper presented at the ESP workshop held in The Woodlands, Texas; April 24e26, 2013

[24] Takacs, G., 2017. Electrical Submersible Pumps Manual. Second ed. Gulf Professional Publishing.

[25] D.A. Chirkov and E.O. Timashe: Efficiency of a submersible plunger pump linear motor 1PNRPU, Perm, Russian Oil company "Rosneft", Moscow, Russian Federation,

[26] Liu, Y ap I: Discussion on several principal problems aroused from measuring high-performance permanent magnetic materials, International Journal of Applied Electromagnetics and Mechanics, vol. 55, no. 3, pp. 453-479, 2017

[27] Brinner TR, McCoy RH, Kopecky T. Induction versus permanent-magnet motors for electric submersible pump field and laboratory comparison. IEEE Transactions on Industry Applications January/February 2014;50(1):174e81.

[28] Takacs, G., 2017. Electrical Submersible Pumps Manual, ” second ed. Gulf Professional Publishing.

[29] Gieras JF. Permanent magnet motor technology. Design and applications. 3rd ed. Boca Raton, USA: CRC Press; 2010

[30] Lex submersible pumps catalog. Ultra-high-speed systems. Lex Submersible Pumps FZE; 2016. Available from: www.lexsp.com

[31] R. Krishnan “Electric Motor Drives Modeling, Analysis, and Control” Pearson Pearson Education 2001

[32] Takacs, G., 2017. Electrical Submersible Pumps Manual, ” second ed. Gulf Professional Publishing

[33] E. C. Lovelace, T.M. Jahns, and J. L. K. a. J. H. Lang, "An Interior PM Starter Alternator for Automotive Applications," in International Conference on Electric Machines and Drives Conference, Istanbul, Turkey, 1998

[34] Tianran He, Ziqiange Zhu: Permanent Magnet Machines for High-Speed Applications World Electr. Veh. J. 2022, 13(1), 18; https://doi.org/10.3390/wevj13010018

[35] E. C. Lovelace, T.M. Jahns, and J. L. K. a. J. H. Lang, "An Interior PM Starter Alternator for Automotive Applications," in International Conference on Electric Machines and Drives Conference, Istanbul, Turkey, 1998.

[36] D.E Rice A detailed analysis of six-pulse converter harmonic currents: IEEE Transactions on Industry Applications (Volume: 30, Issue: 2, March-April 1994)

[37] Brian J. McRee, David A. Dodson. investigation of harmonic distortion in multi-pulse rectifiers for large capacitive charging applications: 2016 IEEE International Power Modulator and High Voltage Conference (IPMHVC)

[38] Haitham Abu-Rub, Atif Iqbal, Jaroslaw Guzinski: High-performance Control of AC Drives with MATLAB/Simulink models.

[39] Fellside F and Wortley A T 1969 Steady-state oscillation and stabilization of variable-frequency inverter fed induction motor drives. Proc. IEEE 116(6): 991–999

[40] Koga K, Ueda R, and Sonoda T 1990 Constitution of V/f control for reducing the steady state speed error to zero in induction motor drive system. In: Proceeding of the IEEE IAS Annual Meeting, vol. 1, pp. 639–646.

[41] Cornell E P and Novotny D W 1972 Theoretical and experimental analysis of operating point stability of synchronous machines. IEEE Trans. Power Apparatus Syst. PAS-91(1): 241–248

[42] Varghese G C, Lang J H, and Casey L F 1986 Analysis of instability in electric machines. IEEE Trans. Ind. Appl. IA22: 853–864

[43] Lipo T A and Krause P C 1967 Stability analysis for variable frequency operation of synchronous machines. IEEE Trans. Power Appl. Syst. 3: 227–234

[44] Kiuchi M, Ohnishi T, Hagiwara H and Yasuda Y 2010 V/f control of permanent magnet synchronous motors suitable for home appliances by DC-link peak current control method. In: Proceedings of the International Power Electronics Conference, pp. 567–573

[45] The Flux-Based Sensorless Field-Oriented Control of Permanent Magnet Synchronous Motors without Integrational Drift. Actuators 2018, 7, 35; doi:10.3390/act7030035

[46] Vas, P. Sensorless Vector and Direct Torque Control; Oxford University Press: Oxford, UK, 1998; ISBN 9780198564652.

[47] M. S. Merzoug, and F. Naceri Comparison of Field-Oriented Control and Direct Torque Control for Permanent Magnet Synchronous Motor (PMSM); World Academy of Science, Engineering, and Technology 21 2008

[48] L. Tang, L. Zhong, M. F. Rahman and Y. Hu, "A Novel Direct Torque Control for Interior Permanent Magnet Synchronous Machine Drive System with Low Ripple in Torque and Flux-A Speed Sensorless Approach" 0-7803-7420-7/02/$17.00 © 2002 IEEE

[49] M. F. Rahnian. L. Zhong. "Comparison of torque response of the interior permanent magnet niotor under PWM current and direct torque control". IEEE, 1999 . p. 1464 - 1470.

[50] Chikh, K., Khafallah, M., Saad, A., Yousfi, D., Chaikhy, H.: A novel fixed-switching-frequency DTC for PMSM drive with low torque and flux ripple based on sinusoidal pulse width modulation and predictive controller. Int Conf. Multimedia. Comput. Syst. (2012). https://doi.org/10.1109/ICMCS.2012.6320189

[51] Utkin, V.I.: Sliding mode control design principles and applications to electric drives. IEEE Trans. Ind. Electron 40, 23–36 (1993)

[52] Wang, A., Jia, X., Dong, S.: A new exponential reaching law of sliding mode control to improve performance of permanent magnet synchronous motor. IEEE Trans. Mag. 49, 2409–2412 (2013)

[53] M. S. Merzoug, and F. Naceri Comparison of Field-Oriented Control and Direct Torque Control for Permanent Magnet Synchronous Motor (PMSM); World Academy of Science, Engineering, and Technology 21 2008

[54] Performance Comparison Between PCB-Stator and Laminated-Core-Stator-Based Designs of Axial Flux Permanent Magnet Motors for High-Speed Low-Power Applications, IEEE Transaction of Industrial Electronics, Vol. 67, No. 7, JULY 2020

[55] L. Tang, L. Zhong, M. F. Rahman and Y. Hu, "A Novel Direct Torque Control for Interior Permanent Magnet Synchronous Machine Drive System with Low Ripple in Torque and Flux-A Speed Sensorless Approach" 0-7803-7420-7/02/$17.00 © 2002 IEEE

[56] J.F Yang; Y. P Dou; X. Qiu; J.W Ling "Research on DTC of Permanent Magnet Synchronous Motor Without Flux Linkage Loop" 2018 21st International Conference on Electrical Machines and Systems (ICEMS)

[57] Kaushik Rajashekara; Atsuo Kawamura; Kouki Matsuse:" Sensorless Control of Ac motor Drives" IEEE ISBN:0-7803-1046-2

[58] J. Liu, T. A. Nondahl, P. B. Schmidt, S. Royak, and T. M. Rowan, "Generalized stability control for open-loop operation of motor drives," IEEE Transactions on Industry Applications, vol. 53, no. 3, pp. 2517– 2525, May 2017.

[59] Haitham Abu-Rub, Atif Iqbal, Jaroslaw Guzinski: High-performance Control of AC Drives with MATLAB/Simulink models

[60] J. Liu, T. A. Nondahl, P. B. Schmidt, S. Royak, and T. M. Rowan, "Generalized stability control for open-loop operation of motor drives," IEEE Transactions on Industry Applications, vol. 53, no. 3, pp. 2517– 2525, May 2017.

[61] Haitham Abu-Rub, Atif Iqbal, Jaroslaw Guzinski: High-performance Control of AC Drives with MATLAB/Simulink models

[62] T. Lixin, Z. Limin, M. F. Rahman, and Y. Hu, "A novel direct torque controlled interior permanent magnet synchronous machine drive with low ripple in flux and torque and fixed switching frequency," Power Electronics, IEEE Transactions on, vol. 19, pp. 346-354, 2004.

[63] D. Ocean, L. Romeral, J.A. Ortega, J. Cusido, and A. Garcia, "Discrete space vector modulation applied on a PMSM motor," 12th International Power Electronics and Motion Control Conference, EPE-PEMC 2006, pp. 320-325, 2006

[64] Gilbert Foo, Saad Sayeed, and M. F. Rahman, "Sensorless direct torque and flux control of an IPM synchronous motor at low speeds and standstill using high-frequency signal injection", Australian Journal of Electrical and Electronics engineering.

[65] Gilbert Foo and M. F. Rahman, “Sensorless direct torque controlled IPM synchronous motor drive over a wide speed range”, Australian Journal of Electrical and Electronics Engineering, vol. 6, no. 2, pp. 121-131, 2009. Electronics Engineering, vol. 6 no. 3, pp. 221-232, 2009.

[66] “A sensorless direct torque control technique for permanent magnet synchronous motors,” in Conf. Rec. IEEE-IAS Annu. The meeting, vol. 1, 1999, pp. 159–164

[67] Gilbert Foo and M. F. Rahman, “Sensorless direct torque and flux controlled IPM synchronous motor drive at very low speed without signal injection”, Industrial Electronics, IEEE Transactions on, vol. 57, no. 1, pp. 395-403, Jan. 2010.

[68] Gilbert Foo and M. F. Rahman, “Direct torque and flux control of an IPM Synchronous motor drive using a backstepping approach”, IET Electric PowerApplications, vol. 3, no. 5, pp. 413-421, Sept. 2009.

[69] Gilbert Foo, “ Senseless direct torque and flux control of interior permanent magnet synchronous motor at very low speeds including standstill ”, Ph.D. Dissertation, University of New South Wales, 2010

[70] Foo, G., Goon, C.S., Rahman, M.F.: ‘Analysis and design of the SVM direct torque and flux control scheme for IPM synchronous motors. Int. Conf. Electrical Machines and Systems, 2009, ICEMS 2009, 2009, pp. 1– 6

[71] L. Chen, K.L. Fang, and Z.F. Hu, "A scheme of fuzzy direct torque control for induction machine," Proceedings of the Fourth International Conference on Machine Learning and Cybernetics, Guangzhou, pp. 803-807, 2005

[72] Emre Ozkop and Halil I. Okumus: Direct Torque Control of induction motor using with Space Vector Modulation. IEEE Xplore. @2008 978-1-4244-1933

[73] Paul C. Krause Oleg Wasynczuk, Scott D. Sudhof: Analysis of Electric Machinery and Drive Systems

[74] J. Feng, W. Gui, J. Xu, and J. Wang, Compare of Permanent Magnet Synchronous Motor Applied to Railway Vehicle Traction System, 2nd IEEE Conference in Industrial Electronics and Applications, pp.74-77, May 2007

[75] X. Liang, N. C. Kar, and J. Liu, “Load filter design method for medium voltage drive applications in electrical submersible pump systems,” IEEE Trans. Ind. Appl., vol. 51, no. 3, pp. 2017–2029, May/Jun. 2015

[76] Xiaodong Liang; Sherif Omar Faried; Obinna Ilochonwu: Subsea Cable Applications in Electrical Submersible Pump Systems. IEEE Transactions on Industry Applications (Volume: 46, Issue: 2, March-April 2010)

[77] L.F. Cruz, " Theoretical Model of Neurobiological Computation to Solve Complex Problems in Higher Education Based on the Sciences of Complexity", Ph.D. dissertation, Janus University, Newport, California, USA, 2012 http://www.eng.usf.edu/~wmoreno/publication.html.

[78] Dennis Harris; Mark Bahman; David Malone: Design and Qualification Testing of ESP Cable to Improve ESP System Run Life. SPE Gulf Coast Section Electric Submersible Pumps Symposium, Paper Number: SPE-194402-MS

[79] A. Ali Qazalbash; Awais Amin; Abdul Manan; Mahveen Khalid; Design and implementation of microcontroller-based PWM technique for sine wave inverter. 2009 International Conference on Power Engineering, Energy and Electrical Drives

[80] Marco Pastura; Stefano Nuzzo; Mario Kohler; Davide Barater: Dv/Dt Filtering Techniques for Electric Drives: Review and Challenges: IECON 2019 - 45th Annual Conference of the IEEE Industrial Electronics Society

[81] R. Dodson and Mulu Woldeyohannes Production Optimization: The Link to Electrical Efficiency in ESP Applications. ©2009 Baker Hughes.

[82] Marco Pastura; Stefano Nuzzo; Mario Kohler; Davide Barater: Dv/Dt Filtering Techniques for Electric Drives: Review and Challenges: IECON 2019 - 45th Annual Conference of the IEEE Industrial Electronics Society

[83] Ralph E. Fehr III University of South Florida: Industrial power Distribution. @2002 by Prentice Hall.

About the Author

Mulu Woldeyohannes was born in Addis Ababa, Ethiopia. She received the B.S. degree in Electrical Engineering from the University of South Florida - Tampa, USA.

Mulu has over nineteen years of experience as a senior Electrical Engineer and related field of Engineering at many industries across the United States. Currently, she is a technical Engineering manager at Baker Hugues Inc in Claremore, Oklahoma, USA. Mulu is also serving as an adjunct professor of Electrical Engineering at the Oral Roberts University in Tulsa, Oklahoma, USA. Mulu loves to spend time with her family and loves to help those who need her assistance.